Multi-Scale Coupling in Ocean and Climate Modeling

Final Report for DOE-99089 submitted by

Zhengyu Liu, Department of Atmospheric & Oceanic Sciences, UW-Madison

Leslie M. Smith, Departments of Mathematics & Engineering Physics, UW-Madsion

and UW-Madison participants

Wei Liu, PhD Student, Department of Atmospheric and Oceanic Sciences

Jai Sukhatme, Post-doctoral Researcher 1/1/06-12/31/08, Department of Mathematics

Mark Remmel, PhD Student, Department of Mathematics

Li Wang, PhD Student, Department of Mathematics

We have made significant progress on several projects aimed at understanding multi-scale dynamics in geophysical flows. Large-scale flows in the atmosphere and ocean are influenced by stable density stratification and rotation. The presence of stratification and rotation has important consequences through (i) the conservation of potential vorticity $q = \boldsymbol{\omega} \cdot \boldsymbol{\nabla}\rho$, where $\boldsymbol{\omega}$ is the total vorticity and ρ is the density, and (ii) the existence of waves that affect the redistribution of energy from a given disturbance to the flow. Our research is centered on quantifying the effects of potential vorticity conservation and of wave interactions for the coupling of disparate time and space scales in the oceans and the atmosphere. Ultimately we expect the work to help improve predictive capabilities of atmosphere, ocean and climate modelers. The main findings of our research projects are described below.

1. Mathematical analysis of the statistical properties of the potential vorticity: Susan Kurien, Leslie Smith and Beth Wingate

Two journal publications have resulted from our analysis of the the two-point correlation of potential vorticity (the potential enstrophy): Kurien, Smith & Wingate, *J. Fluid Mech.* **555**, 121-130 (2006), and Kurien, Wingate & Taylor, *Europhys. Lett.* **84** (2008).

Starting from the Boussinesq equations for rotating and stratified flow, we derive exact scaling laws for the potential enstrophy in two limits. The first limit is for large rotation and stratification describing a range of scales for which vertical stretching by N/f leads to local isotropy (invariance under arbitrary rotations and translations), where N is the buoyancy frequency and f is the Coriolis parameter (twice the background rotation rate). The second limit is for small rotation and stratification, in which the fluid velocity is governed by the isotropic Navier-Stokes equations and the density is a passive scalar. We also identified several regions in parameter space where diffusion and dissipation effects are sub-dominant to nonlinear effects, and thus where one might expect 'inertial-range' transfer characterized by a constant flux of potential enstrophy.

We are working on understanding the constraints that potential enstrophy conservation imposes on the transfer of energy. We have found an exact relation between the two quantities in strongly rotating and stratified flows with equal Rossby and Froude numbers in a unit aspect ratio domain.

The Rossby Ro and Froude Fr numbers may be defined as $Ro = U/(Lf)$ and $Fr = U/(HN)$ where U is a characteristic velocity, H is the vertical scale (in the direction of the rotation/stratification) and L is the horizontal domain scale (in the direction perpendicular to the rotation/stratification). For the unit aspect ratio domain $H = L$. The exact relation between energy and potential enstrophy leads to a prediction for the scaling of the potential energy as a function of the vertical wavenumber ($E_{pe} \propto k_z^{-3}$), and for the scaling of the kinetic energy as a function of horizontal wavenumber ($E_{ke} \propto k_h^{-3}$). These scalings imply that horizontal kinetic energy is suppressed in the small aspect-ratio wavemodes, and potential energy in suppressed in the large aspect-ratio wavemodes. These are the first derived constraints on energy due to potential enstrophy since the landmark results of Charney (1971) for quasi-geostrophic flows. High-resolution numerical simulations of the Boussinesq equations in the relevant parameter regimes show spectral scaling exponent closer to -4, and hence even stronger suppression than is predicted by dimensional estimates. We are concurrently aiming to extend the results to flows which have unequal Rossby and Froude and also to understand such constraints using asymptotic analysis.

2. Self-similarity in decaying two-dimensional stably stratified adjustment. Jai Sukhatme & Leslie Smith

One journal publication has resulted from our study of adjustment in stably stratified, two-dimensional Boussinesq flow: Sukhatme & Smith, *Phys. Fluids* **19**, 036603 (2007).

The evolution of large-scale density perturbations is studied in a stably stratified, two-dimensional flow governed by the Boussinesq equations. As is known, initially smooth density or temperature profiles develop into fronts in the very early stages of evolution (Figure 1). This results in a frontally dominated k^{-1} potential energy spectrum. The fronts, initially characterized by a relatively simple geometry, spontaneously develop into severely distorted sheets that possess structure at very fine scales, and thus there is a transfer of energy from large to small scales (Figure 2). We showed that this process culminates in the establishment of a $k^{-5/3}$ kinetic energy spectrum, although its scaling extends over a shorter range as compared to the k^{-1} scaling of the potential energy spectrum (Figure 3). The establishment of the kinetic energy scaling signals the onset of enstrophy decay, which proceeds in a mildly modulated exponential manner and possesses a novel self-similarity. Specifically, the self-similarity is seen in the time invariant nature of the probability density function PDF associated with the normalized vorticity field (Figure 4). Given the rapid decay of energy at this stage, the spectral scaling is transient and fades with the emergence of a smooth, large-scale, very slowly decaying, almost vertically sheared horizontal mode with most of its energy in the potential component, i.e., the Pearson-Linden regime.

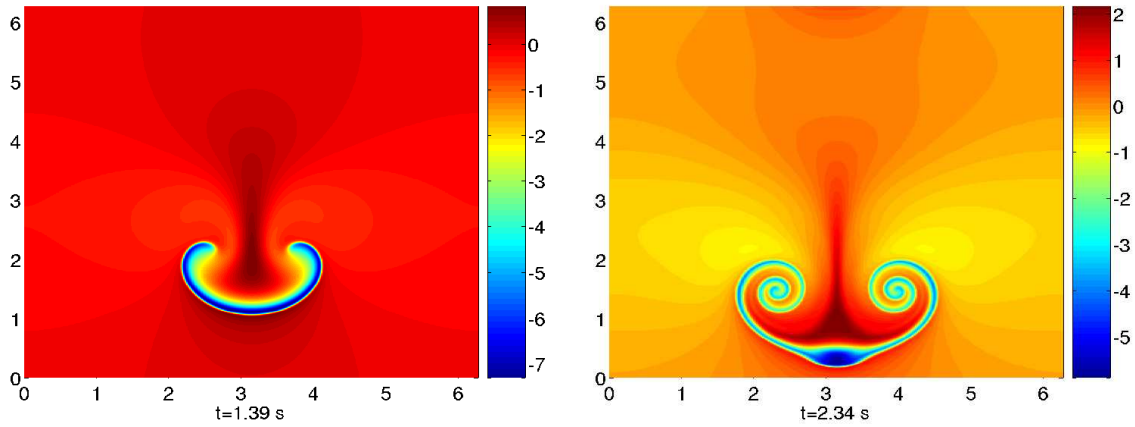

Figure 1: Snapshots of the temperature field at early times.

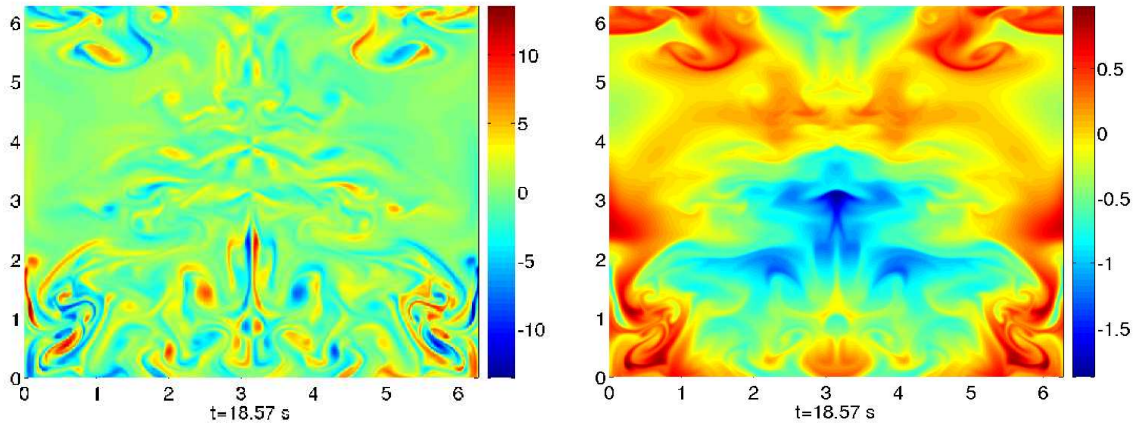

Figure 2: Snapshots of the vorticity (left) and temperature (right) field at a later time when small scales are clearly present.

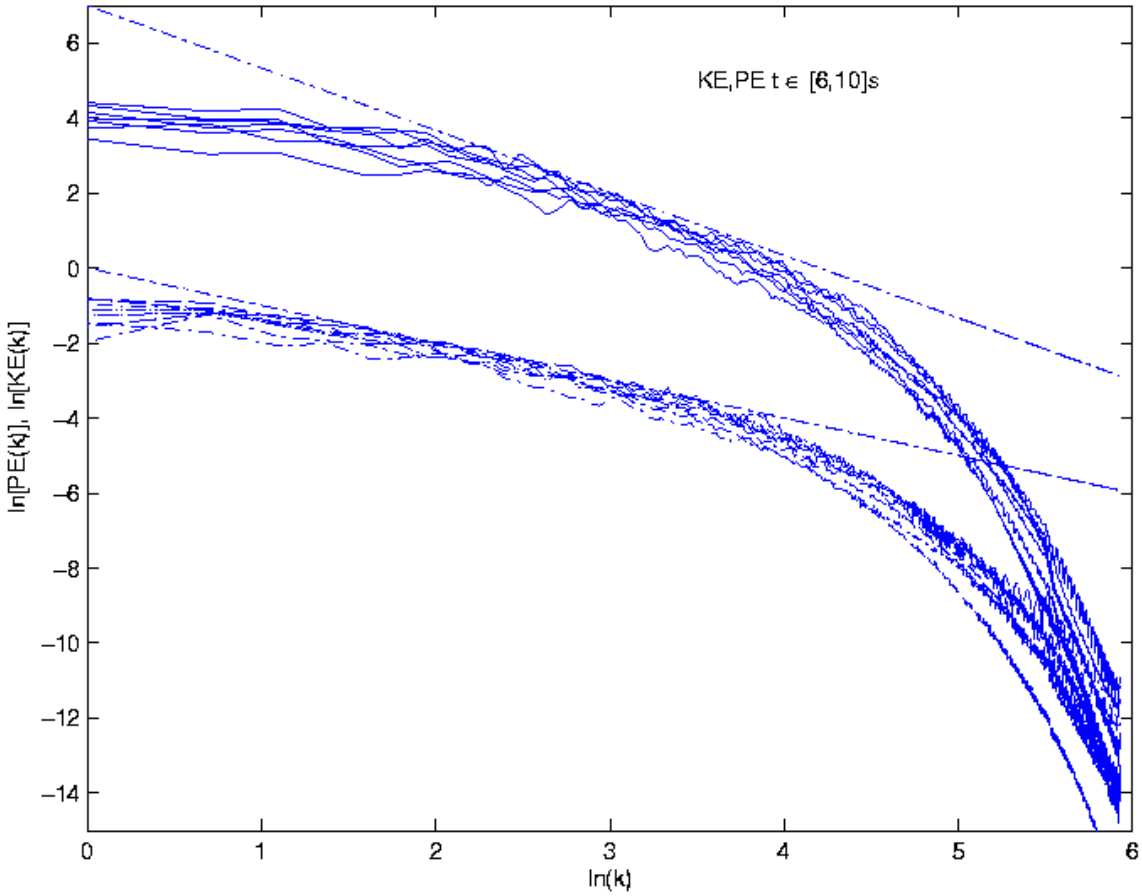

Figure 3: Spectra of the kinetic and potential energy from 1D cuts of the temperature and velocity fields, respectively. The two bunches of curves have been shifted for clarity; the upper bunch shows that the kinetic energy spectra scale as $k^{-5/3}$; the lower bunch shows that the potential energy spectra scale as k^{-1}.

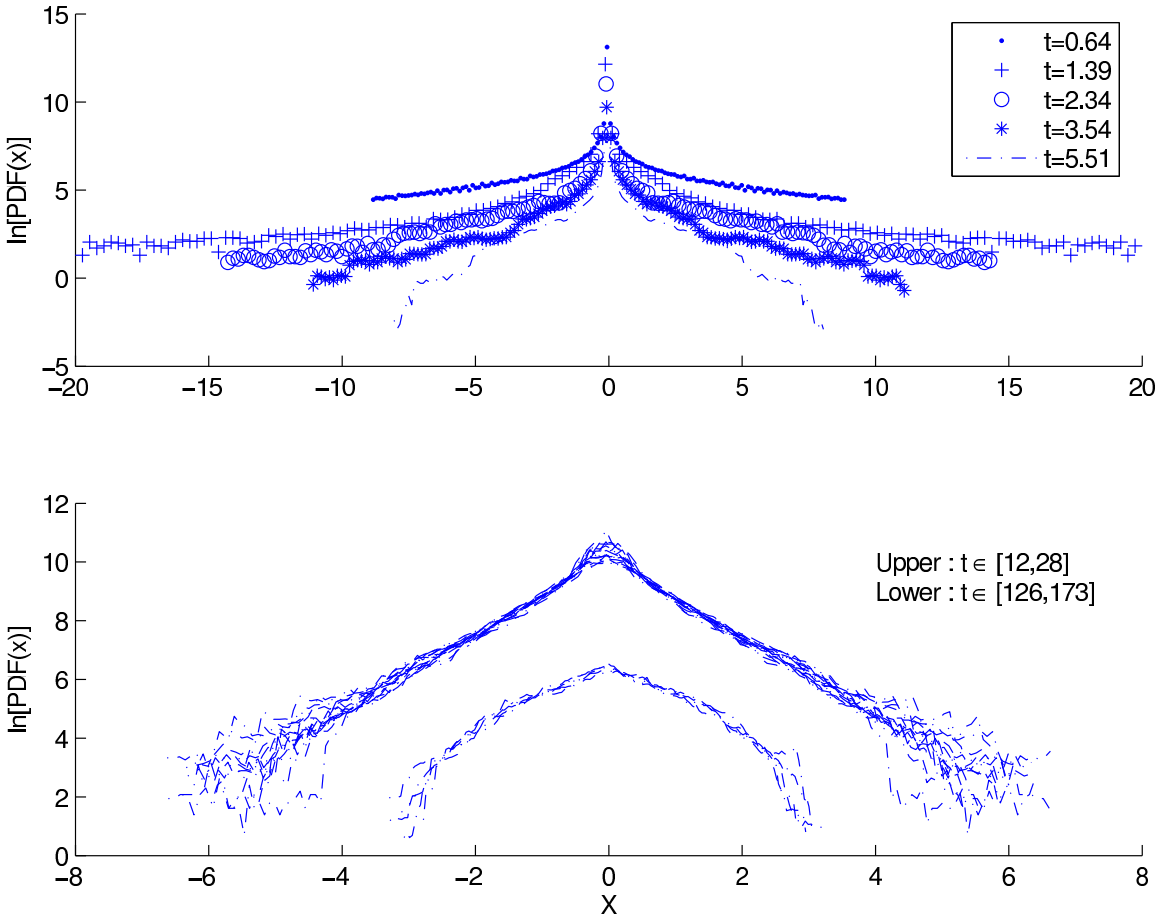

Figure 4: PDFs of the normalized vorticity field. The upper panel shows the approach to a self-similar profile; note the decrease in intermittency with time. The two bunches of curves in the lower panel consist of profiles evenly spanning time in the intervals $[12, 28]$ and $[126, 173]$ seconds, respectively. The upper bunch represents the interval during which the enstrophy decay is exponential in character, whereas the lower bunch shows the PDFs in the Pearson-Linden regime.

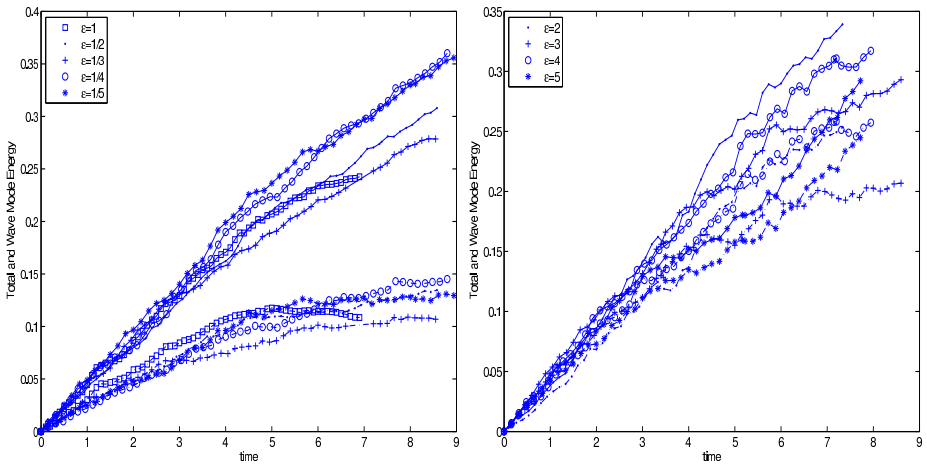

Figure 5: Total and wave energies vs time for $\epsilon = f/N \leq 1$ (left) and $\epsilon > 1$ (right) showing the asymmetry about $\epsilon = 1$.

3. Effects of dispersion on vortical and wave modes in 3D rotating and stratified flows: random large scale forcing. Jai Sukhatme & Leslie Smith

This work has been published in *Geophysical and Astrophysical Fluid Dynamics*, **102** 437-455 (Sukhatme & Smith, 2008).

Utilizing an eigenfunction decomposition, we study the growth and spectra of energy in the vortical (geostrophic) and wave (ageostrophic) modes of a three-dimensional (3D) rotating stratified fluid as a function of dispersion, i.e. of $\epsilon = f/N$, where f, N are the Coriolis parameter and Brunt-Vaisala frequency. Throughout we employ a random large scale forcing in a unit aspect ratio domain and set these parameters such that the Froude and Rossby numbers are roughly comparable and much less than unity. This inquiry is motivated by recent analytical work on the change in character of vortical-wave mode dynamics with dispersion, and especially the asymmetry about $\epsilon = 1$. Looking at the total energy evolution and the wave energy evolution as a function of time, one immediately sees the asymmetry with ϵ (Figure 5). For $\epsilon \leq 1$, the wave energy quickly saturates and the vortical modes energetically dominate for longer times (Figure 5 (left)). For $\epsilon > 1$, the vortical modes contain a small amount of energy and the energy in wave modes continues to grow (Figure 5 (right)).

Stratification stronger than rotation: For $\epsilon = f/N < 1$, the wave mode energy saturates quite quickly. Much like the well understood non-dispersive ($\epsilon = 1$) case (Bartello 1995), the resulting forward cascade continues to act as efficient way of removing ageostrophic energy from the system. Simultaneously, the vortical modes exhibit a pronounced transfer of energy to large scales ($k < k_f$), while the high wavenumber energy spectra associated with the vortical modes scale as k^{-3} for $k_f < k < k_d$. In essence, the picture painted in Bartello (1995) involving the 3D QG dominance of the vortical modes and rapid adjustment via a wave mode cascade is valid for $\epsilon < 1$ (Figure 6 (left)). This picture agrees also with the analytical work by Babin et al. (1997) and Embid & Majda (1998) regarding the splitting of of the vortical and wave modes for $Fr \sim Ro \to 0$ wherein the vortical modes follow 3D QG dynamics while the wave mode cascades are "unfrozen" and result in an efficient transfer of energy to small scales. Interestingly, we observe that dispersive restrictions on the catalytic exact resonances appear to manifest themselves in a steepening of the

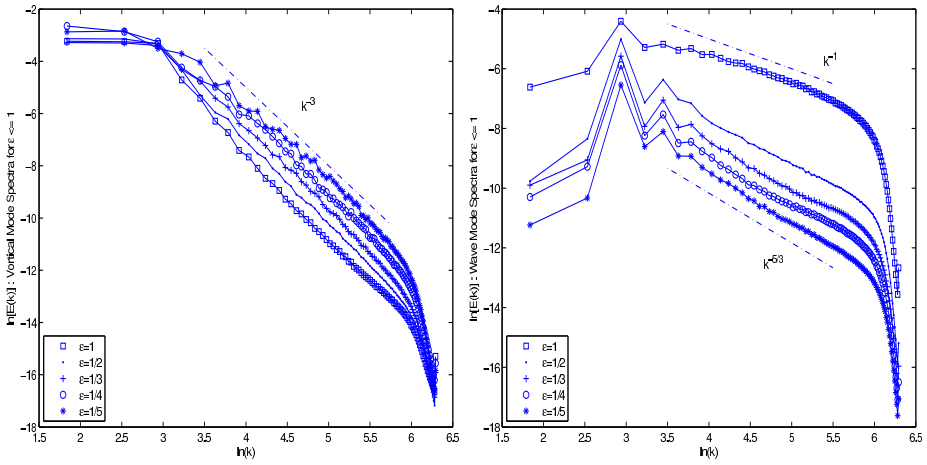

Figure 6: Vortical mode spectra (left) and wave mode spectra (right) for $\epsilon \leq 1$.

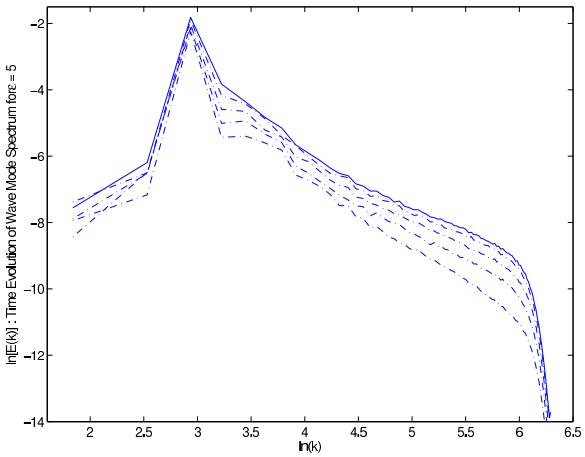

Figure 7: For $\epsilon > 1$, the wave mode energy never saturates and the wave mode spectra shift upwards in time, indicating inefficient transfer of energy to small scales via wave interactions. Spectra shown here are for $\epsilon = 5$.

wave mode cascade from a (nonlocally dominated Batchelor regime passive scalar like) k^{-1} to a (local 3D turbulence like) $k^{-5/3}$ scaling for $k_f < k < k_d$ (Figure 6 (right)). Further, we notice a bias in the partition of energy among the different modes at varying scales. Specifically, the vortical modes contain a large portion of the energy at scales $\sim k_f$ while the wave modes have most of the energy at smaller scales. This naturally introduces a gradual steep-shallow transition in the total energy spectrum. In a broader context, the focus on forward transfers of energy in the present work serves as a counterpart to Smith & Waleffe (2002) wherein small scale random forcing was employed to probe the inverse transfer of energy for the regimes$1/2 \leq \epsilon \leq 2$ and $\epsilon << 1$, and to elucidate the resulting 3D QG or VSHF dominance, respectively.

Rotation stronger than stratification: Proceeding to $\epsilon > 1$, we immediately confirm the asymmetry anticipated from Babin et al. (2002). The wave modes never saturate and soon dominate the entire energy in the system. In spite of this, their spectra do appear to achieve invariance. While shifting upwards, they show signs of a k^{-2} scaling (for larger ϵ values) for an intermediate range of scales $k_f < k < k_r$ where $k_r > k_d$, much like the weak forward cascade in purely rotating turbulence (Figure 7, Cambon et al. 1997, Yeung & Zhou 1998). This situation is in a sense close to the observations for the shallow water equations whereby switching on rotation was seen to inhibit forward transfer (Yuan & Hamilton 1994; see also Farge & Sadourny 1989 for remarks on the difficulty in achieving geostrophic adjustment in a similar scenario). As for $\epsilon \leq 1$, the vortical modes continue to follow 3D QG dynamics though now their role is quite small in that they contain only a small fraction of the total energy in the system. In fact, seeing that the fraction of energy in the vortical modes decreases with increasing ϵ provides some hope that, at least in an energetic sense, the $\epsilon >> 1$ limit of the 3D rotating Boussinesq system will transition smoothly to a purely rotating flow. The scaling of the vortical-mode spectra for $\epsilon > 1$ follows a k^{-3} form for $k_f < k < k_2$ and is followed, for larger values of ϵ, by a shallower form for $k_2 < k < k_d$. Finally, in contrast to $\epsilon \leq 1$, now the wave modes dominate the total energy in the system for all $k > k_f$.

With regard to atmospheric phenomena, recent very high resolution studies of the rotating Boussinesq equations with large scale forcing and $N \gg f$ in a skewed aspect ratio domain show a similar k^{-3} scaling for vortical-mode spectra, $k^{-5/3}$ scaling for wave-mode spectra, and vortical-mode energy dominance at large scales (Kitamura 2006). Indeed, the spectral transitions in the total energy (also in the potential and kinetic energies) that occur quite naturally in the Boussinesq system when $\epsilon < 1$ are reminiscent of the classic synoptic-mesoscale Nastrom-Gage spectrum (Nastrom & Gage 1985). However, it should be kept in mind that the $k^{-5/3}$ portion of the Boussinesq spectra arises from wave modes whereas some observational evidence points to a vorticial mode dominance even at small scales (Cho, Newell & Barrick 1999). Furthermore, as clearly put forth in the recent work of Tulloch & Smith (2006), it is difficult to imagine a consistent theory of the midlatitude tropospere that does not explicity address the potentially complicated evolution of buoyancy (or potential temperature) on domain boundaries (see for example Held et al. 1995 and Sukhatme & Pierrehumbert 2002).

4. Reduced dynamics and an investigation of anticyclone dominance in rotating shallow water flows. Mark Remmel & Leslie Smith.

One manuscript is Remmel, M. & Smith, L.M. 2009 New Intermediate Models for Rotating Shallow Water and an Investigation of the Preference for Anticyclones, *J. Fluid Mech.* **635**, 321-359.

The two-dimensional and three-dimensional quasigeostrophic models (2DQG and 3DQG) are

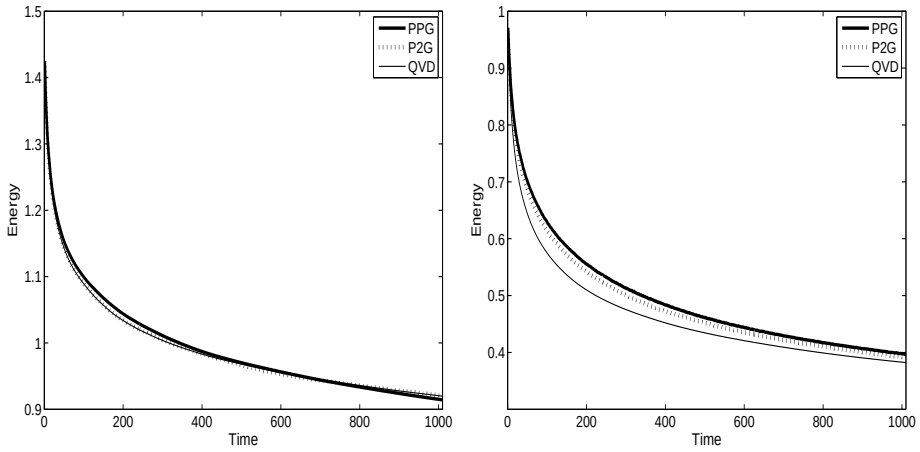

Figure 8: Energy vs time for Ro=.25 and Fr=.2. Left: balanced initial conditions; Right: unbalanced initial conditions.

often used as a starting point to understand rotating and stratified flows. They are simpler and less costly to compute than their 'parent' equations, respectively, the Rotating Shallow Water (RSW) equations and the Boussinesq equations. The 2DQG and 3DQG equations are given by the nonlinear interaction of the non-wave vortical modes of the linearized RSW and Boussinesq systems, and thus do not account for gravity and inertial-gravity wave motions and vortical-wave interactions. The 2DQG and 3DQG equations are known to exhibit symmetry between cyclones and anticyclones, whereas the RSW and Boussinesq systems exhibit strong cyclone/anitcyclone asymmetry in certain parameter regimes.

Whereas previous researchers have derived corrections to QG using perturbative techniques (e.g. Muraki, Snyder & Rotunno 1999, McIntyre & Norton 2000), here we explore reduced models for the RSW equations by including subsets of gravity wave modes in a non-perturbative manner. The method we describe below is general and can be applied to any dispersive wave system for a complete understanding of vortical-wave interactions. For the case of the RSW equations, we are especially interested in determining which vortical-wave interactions are responsible for the dominance of anticylones exhibited by the full RSW equations at moderately small values of the Rossby number (Polvani et al. 1994).

The rotating Shallow-Water equations are (Salmon, 1998)

$$\begin{aligned}
\frac{\partial u}{\partial t} + u\frac{\partial u}{\partial x} + v\frac{\partial u}{\partial y} - fv &= -g\frac{\partial h}{\partial x}, \\
\frac{\partial v}{\partial t} + u\frac{\partial v}{\partial x} + v\frac{\partial v}{\partial y} + fu &= -g\frac{\partial h}{\partial y}, \\
\frac{\partial h}{\partial t} + u\frac{\partial h}{\partial x} + v\frac{\partial h}{\partial y} + (H+h)\left(\frac{\partial u}{\partial x} + \frac{\partial v}{\partial y}\right) &= 0. \qquad (1)
\end{aligned}$$

where the horizontal velocity $\mathbf{u}_h = u(x,y)\hat{\mathbf{x}} + v(x,y)\hat{\mathbf{y}}$, the height of the fluid layer is $H + h(x,y)$, H is constant, the Coriolis parameter is $f = 2\Omega$, Ω is the constant background rotation rate and g is the acceleration of gravity.

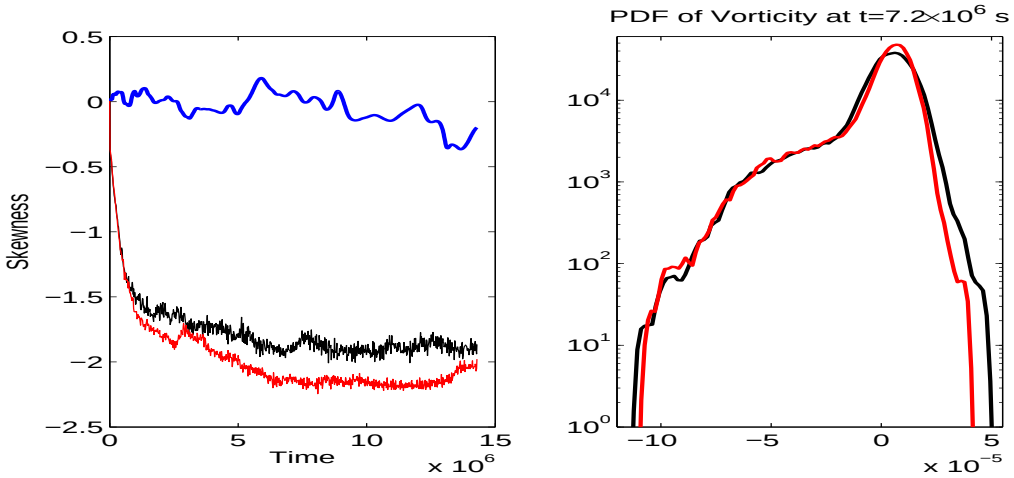

Figure 9: Right: Vorticity skewness vs time in decay from a random field. Black (middle curve): PPG, Red (lower curve): Full RSW, Blue (upper curve): 2DQG. Left: PDF of vorticity at $t = 7.2 \times 10^6$ seconds. Black: PPG; Red: Full RSW.

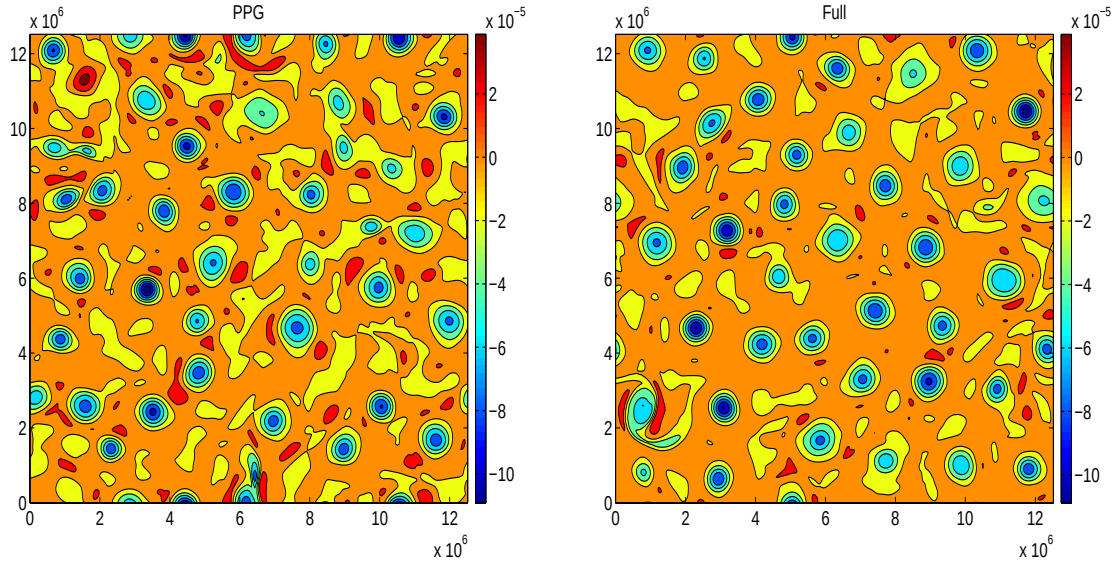

Figure 10: Contours of vorticity at the same time in decay from a random field. Left: PPG reduced model. Right: Full RSW equations. Both the PPG reduced model and the full RSW system show dominance of anticyclones.

For flow with constant f in an unbounded or periodic domain, the linear eigenmodes of the inviscid, unforced equations (1) are Fourier modes

$$\mathbf{v}(\mathbf{x},t) = \boldsymbol{\phi}^m(\mathbf{k}) e^{i(\mathbf{k}\cdot\mathbf{x}-\sigma_m(\mathbf{k})t)} \tag{2}$$

where $\mathbf{v} = [\mathbf{u}_h; h]$ and $\boldsymbol{\phi} = [\hat{\mathbf{u}}_h; \hat{h}]$ and there are three types of modes corresponding to $m = 0, \pm 1$. The $m = 0$ vortical modes are non-wave modes with $\sigma_0(\mathbf{k}) = 0$. There are also two gravity wave modes with $m = \pm 1$ and wave frequency $\sigma(\mathbf{k})$ given by the dispersion relation

$$\sigma_\pm^{SW}(\mathbf{k}) = \pm(f^2 + c^2\, k_h^2)^{1/2} \tag{3}$$

where $\mathbf{k}$ is a vector with components (k_x, k_y), $k = |\mathbf{k}|$, $k_h = (k_x^2 + k_y^2)^{1/2}$ is the horizontal wavenumber and $c^2 = gH$. Since the eigenmodes are orthogonal and complete, the solution to (1) may be written as a superposition of the linear eigenmodes $\boldsymbol{\phi}^m(\mathbf{k})$ with amplitudes $a_m(\mathbf{k}, t)$:

$$\mathbf{v}(\mathbf{x},t) = \sum_{\mathbf{k}} \sum_m a_m(\mathbf{k},t)\boldsymbol{\phi}^m(\mathbf{k}) \exp[i(\mathbf{k}\cdot\mathbf{x} - \sigma_m(\mathbf{k})t)]. \tag{4}$$

Thus, in Fourier space, equation (1) takes the form

$$\frac{da_m(t;\mathbf{k})}{dt} = \sum_{\mathbf{k}+\mathbf{p}+\mathbf{q}=0} \sum_{n,l} C^{mnl}_{\mathbf{kpq}}\, a_n^*(\mathbf{p},t) a_l^*(\mathbf{q},t)\; e^{i(\sigma_m(\mathbf{k})+\sigma_n(\mathbf{p})+\sigma_l(\mathbf{q}))t}, \tag{5}$$

where $()^*$ denotes the complex conjugate, and nonlinear interactions are among triads with $\mathbf{k}+\mathbf{q}+\mathbf{p} = 0$. Notice that there are twenty-seven types of interactions $\sum_{n,l} C^{mnl}_{\mathbf{kpq}}\, a_n^*(\mathbf{p},t) a_l^*(\mathbf{q},t)$ if one considers all $m, n, l = 0, \pm 1$.

The 2DQG model results from allowing only interactions between the non-wave modes $\boldsymbol{\phi}^0(\mathbf{k})$, and does not include any interactions with wave modes $\boldsymbol{\phi}^+(\mathbf{k})$ or $\boldsymbol{\phi}^-(\mathbf{k})$. We denote the 2DQG interactions between non-wave modes as $(0,0,0)$ interactions. However, there are twenty-six other kinds of interactions that one could include in a new model. It is natural to consider first the class of interactions between two non-wave modes and one wave modes, denoted $(0,0,+)$ and $(0,0,-)$ interactions (and all permutations). We call the new model PPG:

$$\frac{\partial Q}{\partial t} + J(Q,\psi) + Q\nabla^2\chi + \nabla Q\cdot\nabla\chi = 0$$

$$\frac{\partial(f\nabla^2\psi - g\nabla^2 h)}{\partial t} - c^2\nabla^4\chi + f^2\nabla^2\chi = fgH\; J((f^2 - c^2\nabla^2)^{-1}Q, Q)$$

$$\frac{\partial\nabla^2\chi}{\partial t} + g\nabla^2 h - f\nabla^2\psi = 0 \tag{6}$$

where $\nabla^2\psi = v_x - u_y$ and $u_x + v_y = \nabla^2\chi$ (so $u = \chi_x - \psi_y$ and $v = \chi_y + \psi_x$) and and the quantity $Q = (\nabla^2\psi - fh/N)$ is the linear potential vorticity. This model may be compared to potential vorticity inversion models in which wave amplitudes are slaved to the vortical modes (e.g., Muraki, Snyder and Rotunno 1999, McIntyre & Norton 2000).

Adding to the reduced PPG model all interactions involving one non-wave mode and two gravity wave modes – $(0, \pm, \pm)$ and all permutations – the next model in the hierarchy is denoted P2G. In this manner, one can construct models to investigate the contribution to the full dynamics of any subset(s) of wave-vortical interactions, including three-wave interactions in isolation. As an

example, we compared 2DQG, PPG, P2G and the full RSW equations for decay from balanced and unbalanced initial conditions (Figure 8). For moderate values of the Rossby and Froude numbers $Ro, Fr \approx 0.1$, the full RSW system develops vortices with a strong preference for anticylones as indicated by the development of a negative skewness of vorticity (Figures 9-10, Polvani et al. 1994). Here the Froude number is defined by $Fr = U/(gH)$. As already mentioned, the 2DQG model does not show significant asymmetry between cyclones and anticyclones (Figure 9)). We found that by adding vortical-wave interactions involving a single gravity wave to the 2DQG model, the resulting PPG model captures the asymmetry of the full RSW model remarkably well for (i) decay from balanced initial conditions, and (ii) decay from unbalanced initial conditions with divergence-free velocity field (Figures 9-10). In these cases, the evolution of the skewness for the PPG model and the full RSW system are quantitatively similar. Three-wave interactions were found to be important only for initial velocity field containing significant divergence, in which case the skewness of the full RSW equations becomes more negative than the skewness of the PPG and P2G models at these moderate parameter values.

We have derived the corresponding "corrections" to 3DQG by building a hierarchy of reduced models including more and more vortical-wave interactions starting from the linear eigenmodes of the 3D Boussinesq equations. This method of deriving reduced models in non-perturbative and the corrections are not small.

5. Reduced dynamics of inertia-gravity waves for the 3D rotating Boussinesq equations. Mark Remmel, Leslie Smith & Jai Sukhatme.

One manuscript is *to appear in Communications in Mathematical Sciences*: Remmel, M., Sukhatme, J. & Smith, L.M. 2009, Nonlinear inertia-gravity wave-mode interactions in three-dimensional rotating stratified flows.

Following the derivation procedure outlined in the previous section, we derived a reduced model, denoted GGG, describing nonlinear interactions between intertia-gravity waves $(\pm, \pm, \pm)$ of 3D rotating Boussinesq flow, in the absence of interactions with vortical modes. For brevity, we do not present the GGG equations here, but refer the reader to the manuscript (to appear and available upon request). Our first investigation of the GGG model focused on strongly stratified and strongly rotating flows with comparable stratification and rotation strengths, i.e. flow with order one Burger number $Bu = Fr^2/Ro^2 \approx 1$ with $Fr = U/(NH)$, $Ro = U/(fL)$ and $Fr \approx Ro \ll 1$. Furthermore, as in most atmosphere-ocean phenomena, we considered small-aspect-ratio domains with height to length ratio $H/L < 1$. One goal is to determine which interactions are primarily responsible for the scaling of wave-mode energy. We present results from two sets of parameters: (i) $Fr = Ro \approx 0.1$, $H/L = 1/3$, and (ii) $Fr = Ro \approx 0.05$, $H/L = 1/5$. In both cases, an external random force is applied to large scales in order to explore the possibility of a long-time forced-dissipative statistically steady state. In comparison cases of the full Boussinesq dynamics, the vortical modes are damped at large scales since they support an inverse cascade for $Bu = O(1)$ with $Ro \approx Fr \ll 1$ (Babin et al. 2000).

For the first set of parameters $Ro = Fr \approx 0.1$ and $H/L = 1/3$, Figure 11 compares energies in time (right) and wave-mode energy spectra at time $t = 17.7$ (left) for the GGG model and the full Boussinesq system. The large-scale random force is applied only to wave modes and is therefore identical for both systems. Both systems appear to approach a quasi statistically steady state. One can see that the (wave-mode) energy of the GGG model is higher than the total energy of the full

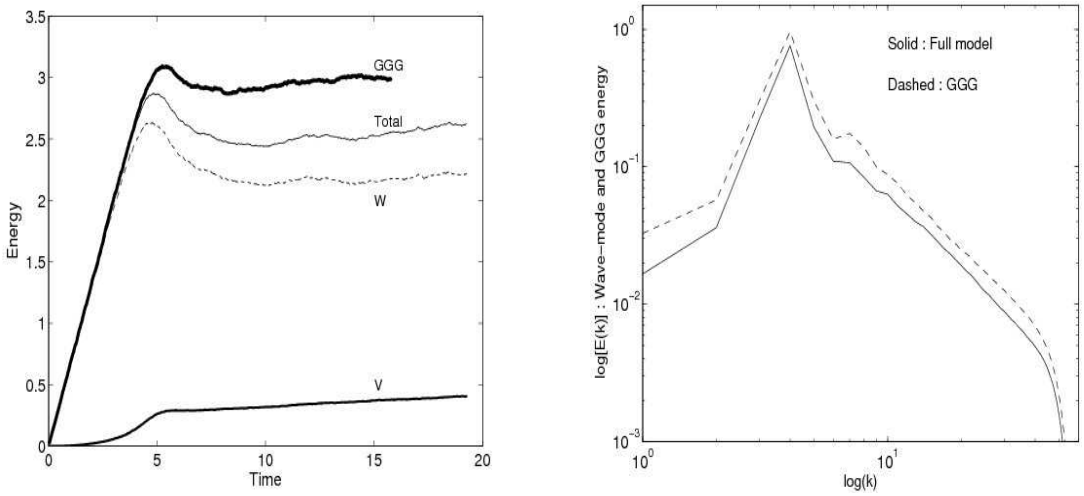

Figure 11: The GGG model compared to the full Boussinesq dynamics with $H/L = 1/3$, $Ro = Fr = 0.1$, 162×486^2, identical IG-mode forcing. Left: Energies in time; Right: Wave-mode energy spectra at time $t = 17.7$.

equations, owing to the fact that interactions involving vortical modes are absent from the GGG model. More specifically, near-resonant interactions between two wave modes and one vortical mode in the full system help to transfer energy downscale (Bartello 1995, Sukhatme and Smith 2008). However, the scaling of the wave-mode energy spectra of the GGG and full models appear to be identical when forcing is applied only to wave modes. Thus we conclude that three-wave interactions play an important role to establish the scaling of the wave-mode energy spectrum of the Boussinesq equations under the influence of unbalanced, high-frequency forcing at large scales.

For the second set of parameters, $Ro = Fr \approx 0.05$ and $H/L = 1/5$, Figure 12 shows energies in time at the highest resolution we could achieve (100×500^2 Fourier modes). When only wave modes are forced (left), one sees that GGG and full model energies grow in time and neither simulation approaches a quasi statistically steady state. These results strongly suggest that three wave interactions are under-resolved in both cases. On the other hand, when all modes are forced, the wave-mode, vortical-mode and total energies of the full Boussinesq system approach a constant value as time increases, indicating approach to a forced-dissipative quasi statistically steady state (right plot of Figure 12). Even though three-wave interactions are probably under-resolved, they are a now a secondary effect because the vortical mode energy dominates and the wave-vortical-wave interactions efficiently transfer energy downscale. Nevertheless, the secondary effect of the three-wave interactions (when they are resolved) is likely to change the scaling of the total and wave-mode spectra at high wavenumbers (Figure 13). Thus, larger resolutions are necessary to obtain accurate spectral scalings. This work serves as a caution for most present-day calculations of atmosphere-ocean dynamics in small-aspect ratio domains with $H/L \ll 1$ since we demonstrate that the three-wave interactions are likely under-resolved.

In strongly stratified flow at large Burger number, our investigation of the GGG model is relevant to many recent studies of three-wave interactions as a possible explanation for the Garrett-Munk (1979) spectrum observed in the oceans. Whereas previous investigators (e.g. McComas & Bretherton 1977, Lvov, Polzin & Tabak 2004) have included only exact resonances, our PDE reduced model keeps all 3-wave interactions (exact, near-resonant and non-resonant). The central

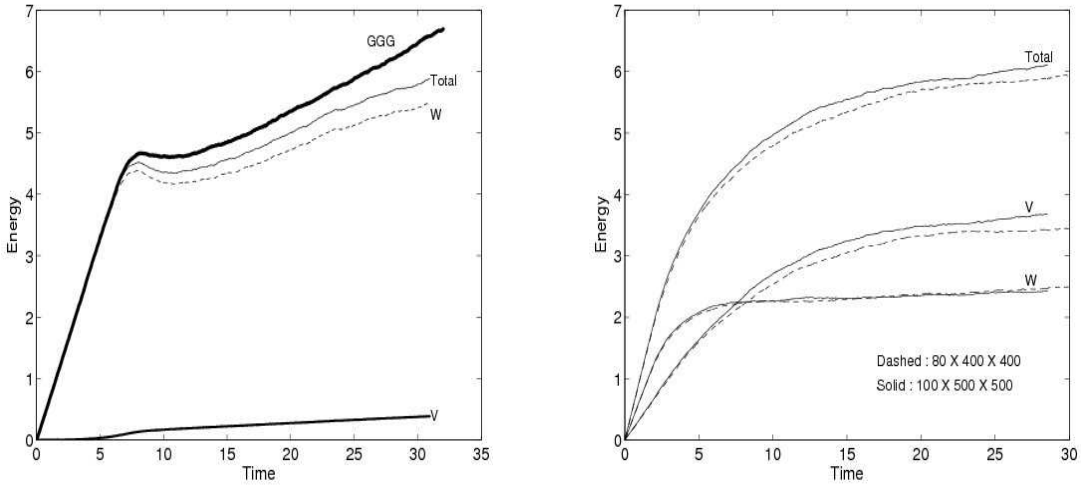

Figure 12: Energies in time for $Fr = Ro \approx 0.05$, $H/L = 1/5$. Right: GGG and full Boussinesq systems with forcing applied only to wave modes, resolution 100×500^2. Left: Full Boussinesq system with forcing applied to all modes, resolutions 80×400^2 and 100×500^2.

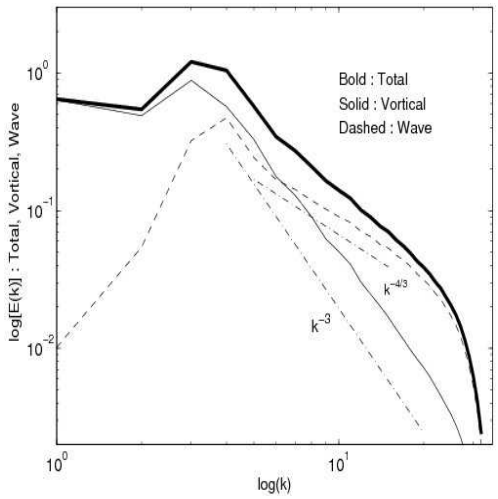

Figure 13: Energy spectra for the full Boussinesq system with $Fr = Ro \approx 0.05$, $H/L = 1/5$, resolution 100×500^2, all modes forced randomly at large scales. High-wavenumber spectral scalings are likely incorrect since 3-wave interactions are under-resolved.

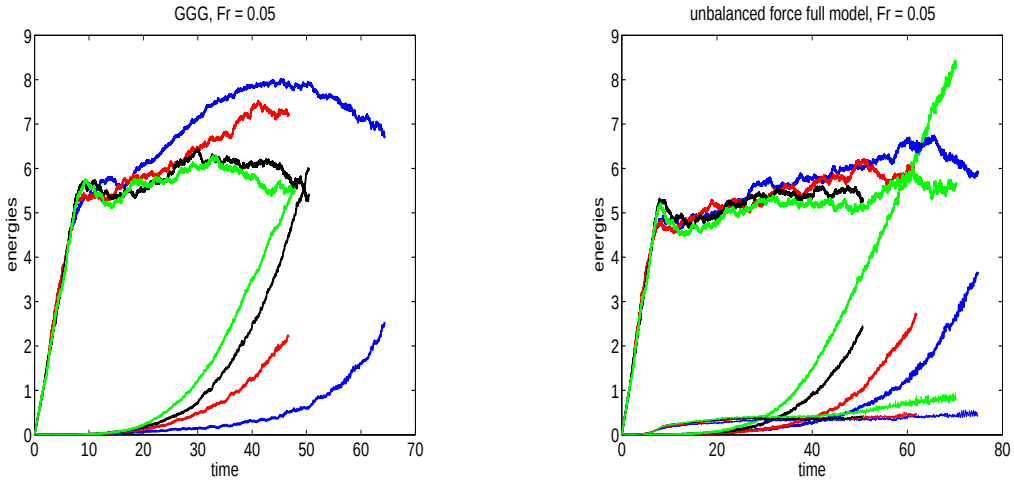

Figure 14: VSHF and wave energies vs time for different resolutions (blue 128^3, red 162^3, black 192^3, green 256^3). Left: GGG model; Right: Full Boussinesq system. In both cases, forcing is applied only to wave modes (not including VSHF modes or vortical modes). Curves showing continuous growth in time correspond to VSHF modes, while curves leveling off and eventually decreasing in time correspond to true wave modes. On the right, the curves with very small amplitude correspond to vortical modes.

question is whether or not the three-wave interactions among inertia-gravity waves in isolation from the vortical modes can explain the Garrett-Munk spectrum, as has been commonly assumed. To answer this question, we compare simulations of the full Boussinesq system to simulations of the GGG model.

With $Fr = 0.05$ in the purely stratified case, Figure 14 shows energies in time for different resolution simulations of the GGG model (left) and the full Boussinesq system (right). In both cases, forcing is applied only to true wave modes, while modes with zero frequency are not forced directly. The zero-frequency modes are (i) vertically sheared horizontal flows (VSHF, the limiting case of wave modes for vanishing horizontal wavenumber), and (ii) vortical modes. Curves showing continuous growth in time correspond to VSHF modes, while curves leveling off and eventually decreasing in time correspond to wave modes. On the right, the curves with very small amplitude correspond to vortical modes (present in the full system but not present in the GGG model). One can see that neither the GGG nor full model simulations are yet resolved with respect to near-resonant interactions, since the results continue to change as the resolution is increased. The resolution problem persists even when vortical modes are force in addition to true wave modes, but VSHF modes are not directly forced (see Figure 15).

Nevertheless, despite resolution issues, one may investigate the scaling of the GGG wave-mode energy spectra, keeping in mind that higher-resolution simulations will be necessary for increased confidence in the results. Since the true wave-mode energy does not have an extended flat portion, we measured spectra at many single-time snapshots in order to assess the degree of change. Figure 16 (left) shows that the GGG wave-mode energy spectra scale approximately as k^{-2} for a large range of times. Figure 16 (right) shows that the GGG spectra $E(k_z)$ averaged over horizontal wavenumbers k_h exhibit a clean k_z^{-2} scaling, at least for some range of times (the plot is for time $t = 49.3$)). Many intriguing questions remain for future investigation. What is the dependence on

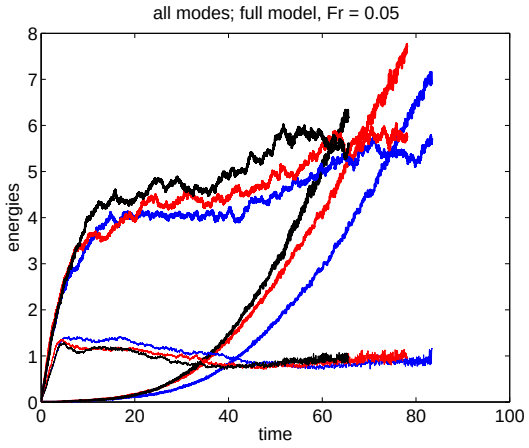

Figure 15: Energies vs time for different resolutions (blue 128^3, red 162^3, black 192^3) of the full Boussinesq system. Forcing is applied only to true wave modes and vortical modes (but not to VSHF modes). Curves showing continuous growth in time correspond to VSHF modes, while upper curves leveling off in time correspond to true wave modes. Lower curves with very small amplitude correspond to vortical modes.

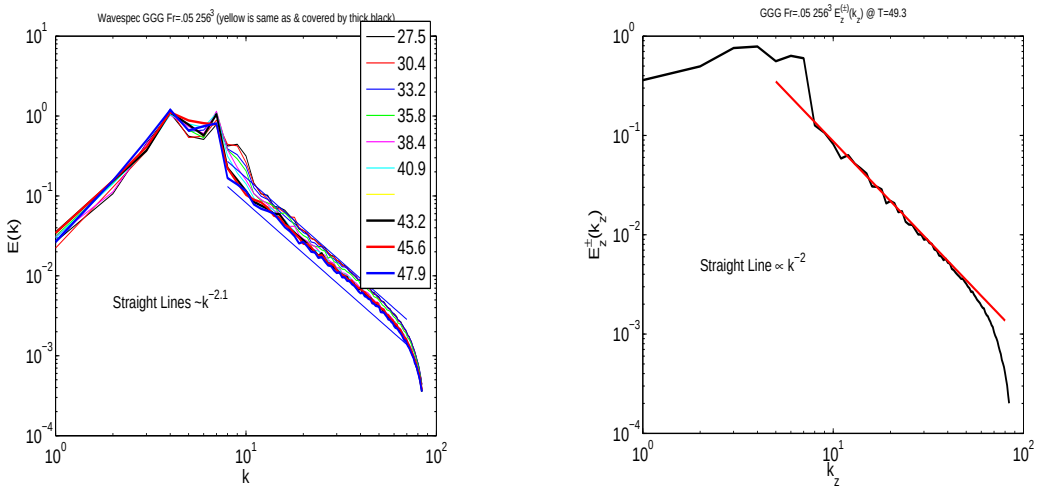

Figure 16: GGG spectra for $Fr = 0.05$ at resolution 256^3. Left: $E(k)$ at many single time snapshots. Right: $E(k_z)$ averaged over k_h at time $t = 49.3$ exhibiting Garrett-Munk scaling k_z^{-2}.

the Froude number, and the effect of the hydrostatic approximation? What is the effect of rotation? Are vortical modes significant as $Fr \to 0$? Is a statistically steady state achieved if VSHF modes are damped? What is the time evolution of spectra, and for what range of times and parameters does the Garrett-Munk scaling persist?

6. Reduced models for β-plane and purely rotating 3D flows. Li Wang & Leslie Smith.

A manuscript is in preparation for journal submission.

For the cases of 3D pure rotation and 2D flow on the β-plane, there is no slow vortical mode solution to the linearized equations. However, there are wave modes. The dispersion relation for the wave frequency takes the value zero for certain wavevectors, and thus there are slow wave modes in both cases.

For 3D flow rotating about the $\hat{\mathbf{z}}$-axis, the wave frequency is given by

$$\sigma^R_\pm = \pm f \frac{k_z}{k}, \quad \mathbf{k} = k_x\hat{\mathbf{x}} + k_y\hat{\mathbf{y}} + k_z\hat{\mathbf{z}} \tag{7}$$

and the slow wave modes with $k_z = 0$ correspond to vortical columns. In a manner similar to Project 4 above, one can investigate the dynamical effect of different subsets of interactions. For example, nonlinear interactions of the slow wave modes in isolation lead to a reduced model consisting of 2D Navier Stokes flow for $u(x,y)\hat{\mathbf{x}} + v(x,y)\hat{\mathbf{y}}$, and this 2D flow advects the vertical velocity $w(x,y)\hat{\mathbf{z}}$ as a passive scalar. However, this model has cyclone/anticyclone symmetry, whereas the full 3D equations generate large-scale cyclones (e.g., Smith & Waleffe 1999). It has been shown by Smith & Lee (2005) that near-resonant interactions with $|\sigma^R_\pm(\mathbf{k}) + \sigma^R_\pm(\mathbf{p}) + \sigma^R_\pm(\mathbf{q})| = Ro < 1$ and $\mathbf{k} + \mathbf{p} + \mathbf{q} = 0$ are responsible for the formation of large-scale cyclones from small-scale random forcing. However, it is not yet clear if those near-resonances are of the type $(0, \pm, \pm)$ or $(\pm, \pm, \pm)$, where here a zero mode is a zero wave mode. The triplet notation here implies all permutations of the triplet. We can this question using reduced models including $(0, 0, 0)$ and $(0, \pm, \pm)$.

A simpler case is the β-plane model for 2D motion on the surface of a sphere a mid-latitudes, accounting for the latitude variation of the Coriolis parameter. In terms of the streamfunction Ψ, the β-plane equation is written

$$\partial_t \nabla^2\Psi + \beta\partial_x\Psi + J(\Psi, \nabla^2\Psi) = \nu\nabla^4\Psi + f \tag{8}$$

where the zonal flow is $u = \partial\Psi/\partial y$, the meridional velocity is $v = -\partial\Psi/\partial x$, and f is an external force.

In the absence of external forcing and in a periodic domain,the inviscid,linear limit of (8) has wave solutions of the form

$$\Psi(\mathbf{x}, t; \mathbf{k}) = \exp(i(\mathbf{k}\cdot\mathbf{x} - \sigma^\beta(\mathbf{k})t)) + c.c, \quad \sigma^\beta(\mathbf{k}) = -\beta\frac{k_x}{k^2}$$

and slow wave modes are zonal flows with $k_x = 0$. The solution $\Psi(\mathbf{x}, t)$ may be represented as a superposition of linear waves, formally written as

$$\Psi(\mathbf{x}, t) = \sum_{\mathbf{k}} a(\mathbf{k}; t)e^{i\mathbf{k}\cdot\mathbf{x}} \tag{9}$$

with reality condition $a(t;\mathbf{k}) = a^*(t;-\mathbf{k})$. Substituting (9) into (8) gives

$$k^2\partial_t a_k + i\beta k_x a_k = \sum_{\mathbf{k}+\mathbf{p}+\mathbf{q}=0} C_{kpq} a^*(\mathbf{p}) a^*(\mathbf{q}) \tag{10}$$

where $C_{kpq} = (q^2 - p^2)(\mathbf{p} \times \mathbf{q}) \cdot \hat{z}$.

On the β-plane, there is no energy transfer between three slow waves with $k_x = 0$, and furthermore, interactions between two slow waves and one fast wave do not exist since they do not form a triad with $\mathbf{k} + \mathbf{p} + \mathbf{q} = 0$. Thus an interesting subset of interactions involving any slow mode is between one slow mode and two fast waves, which we may denote (0,-,-), following the notation of Section 4. Considering all such interactions, we derive the reduced model

$$\partial_t \overline{\Psi_y} + \overline{J(\Psi, \Psi_y)} = 0 \tag{11}$$

$$\frac{\partial}{\partial t}\nabla^2\Psi' + \beta\Psi'_x = \frac{1}{2}\overline{\Psi}_y(\frac{\partial}{\partial x}\nabla\Psi') - \frac{1}{2}\frac{\partial}{\partial y}(\nabla\overline{\Psi})\Psi'_x \tag{12}$$

where $\overline{\Psi}$ denotes the zonal flow with $k_x = 0$ and Ψ' denotes the part of the streamfunction field with $k_x \neq 0$.

However, to make an analogy with 3D rotation where three 2D slow modes with $k_z =$ can interact as a 2D subsystem, one may make a modification of (12). Let us divide modes into near-zero S with wavevectors in a sector $k_x/k_y \leq \delta Rh$, and modes P with wavevectors $k_x/k_y > \delta Rh$, where the Rhines number $Rh = U/(L^2\beta)$. Now the model (S,S+P,S+P) (and all permutations) includes (S,S,S) interactions and (S,P,P) interactions. This model is analogous to the model we would like to study for 3D rotation (0,0,0) together with $(0,\pm,\pm)$. Note that three-wave interactions are excluded and hence we can discern their importance for zonal flow formation in 2D, and cyclonic vortical column formation in 3D, by comparison of the reduced model to full simulations. Of course here for the beta-plane problem we have introduced a new parameter δ as the size of the sector characterizing "near-zero." There is no such parameter in the 3D problem.

The broadened model including dissipation may be written as

$$\partial_t \nabla^2\Psi_s + \beta\partial_x\Psi_s + J_s(\Psi, \nabla^2\Psi) = \nu\nabla^4\Psi_s$$

$$\partial_t \nabla^2\Psi + \beta\partial_x\Psi + \frac{1}{2}(J(\Psi_s, \nabla^2\Psi) + J(\Psi, \nabla^2\Psi_s)) = \nu\nabla^4\Psi \tag{13}$$

where subscript s restricts the function or operator inside the sector about $k_x = 0$. As a warm-up for the 3D problem, we compare simulations of (13) with $Rh = 0.3$ and $\delta = 1.5$. The calculations are performed in a 2π periodic box with resolution 384^3 Fourier modes. Hyperviscosity is used instead of normal viscosity. The system is forced by white-noise with spatial correlation function

$$F(k) = \epsilon_f \frac{\exp(-0.5(k - k_f)^2)}{(2\pi)^{1/2}}$$

where all forced wavevectors satisfy $k_x/k_y > \delta Rh$ and the peak wavenumber is $k_f = 75$. For the parameter values $Rh = 0.3$ (based on forcing parameters) and $\delta = 1.5$, large-scale zonal flows develop. Figure 17 compares maximum westward zonally averaged velocity (blue) to maximum

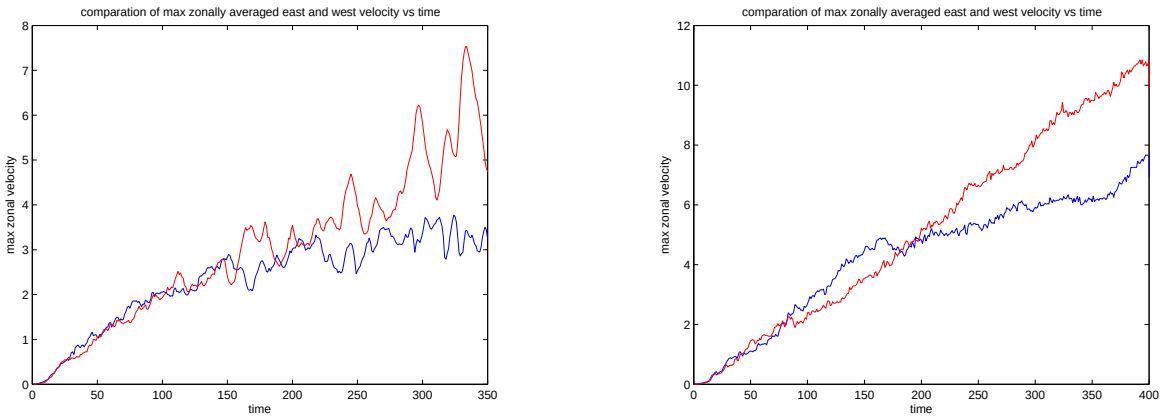

Figure 17: Maximum westward (red) and eastward (blue) zonally averaged velocity as a function of time for a full simulation (left) and the model (13) (right).

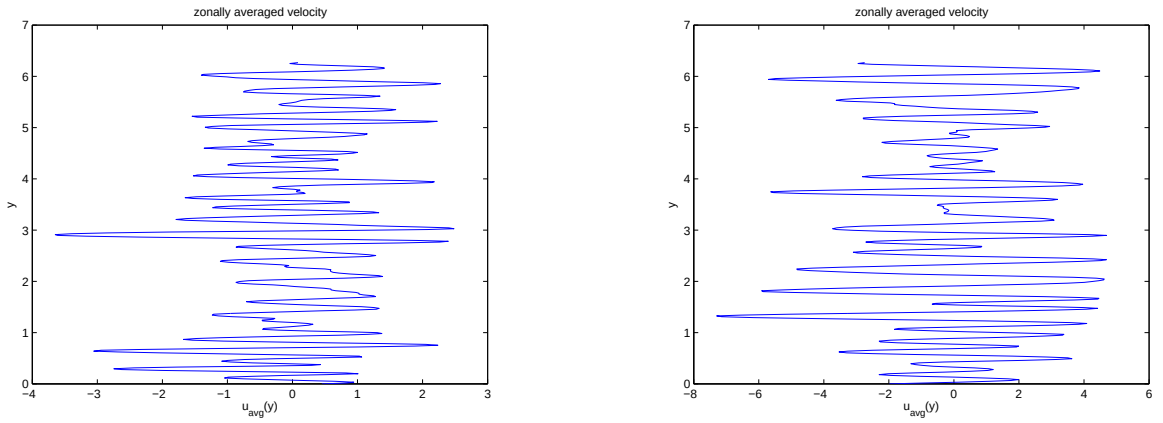

Figure 18: Zonally averaged velocity at time $t = 350$ for the full simulation (left) and the model (13) (right).

eastward zonally averaged velocity (red) as a function of time for the full equations (left) and the model (13) (right). One can see that the model preserves the important asymmetry between eastward and westward zonal flows in favor of stronger westward flows. The important asymmetry to capture in the 3D rotation problem is asymmetry between cyclones and anticyclones in favor of cyclones. Figure 18 compares the zonally averaged velocities at a single snapshot in time ($t = 350$).

Returning to the 3D rotation problem, we investigate the role of $(0, \pm, \pm)$ and three-wave $(\pm, \pm, \pm)$ interactions in the formation and dominance of cyclones. Our results are consistent with earlier work by Lee and Smith (2005) elucidating the importance of near resonances, but go beyond that work to show that the $(0, \pm, \pm)$ near-resonant interactions primarily responsible cyclone/anticyclone asymmetry in favor of cyclones. All results shown here are for Rossby number $Ro = 0.08$ and resolution 128^3 Fourier modes. We are currently extending the results to higher resolution 256^3 Fourier modes and a range of Rossby numbers.

Figures 19 and 20 show that the reduced model including $(0, 0, 0)$ and $(0, \pm, \pm)$ interactions

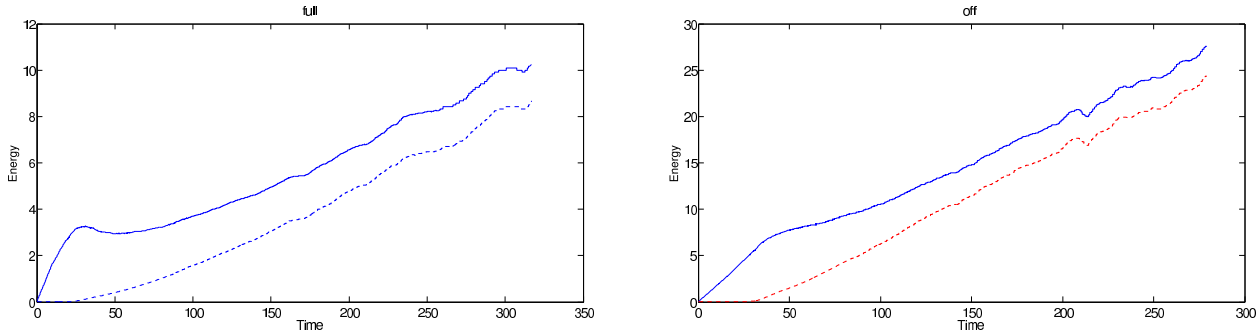

Figure 19: Total energy (solid) and energy in the 2D $k_z = 0$ modes (dash) vs time for the full 3D rotating system (right) and the reduced model including $(0,0,0)$ and $(0,\pm,\pm)$ interactions (left).

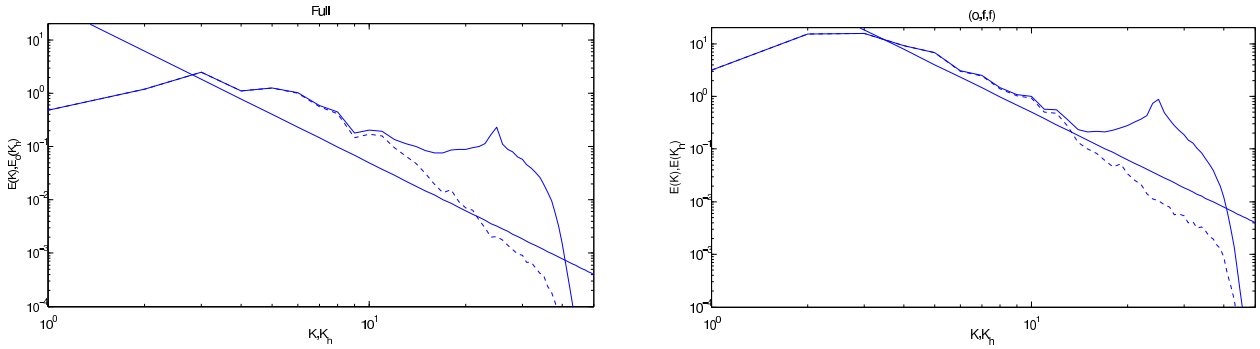

Figure 20: Spectra of total energy (solid) and 2D energy (dash) for the full 3D rotating system (right) and the reduced model including $(0,0,0)$ and $(0,\pm,\pm)$ interactions (left).

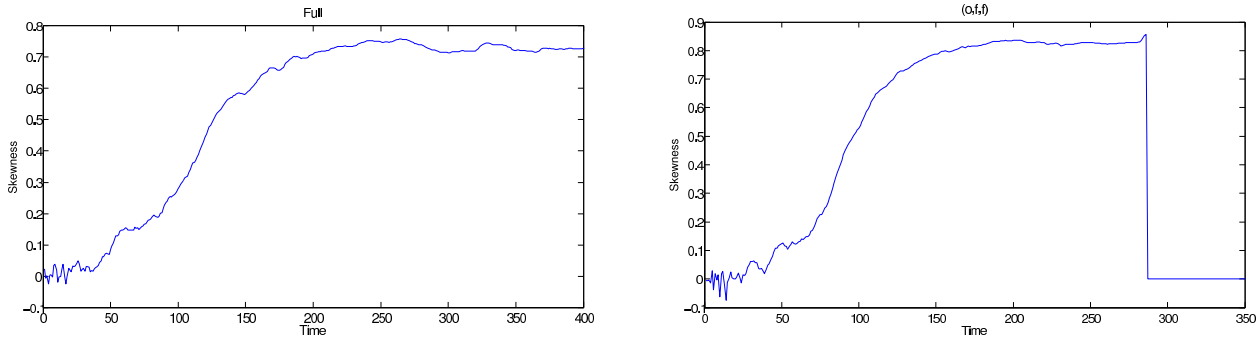

Figure 21: Skewness of vorticity vs time for the full 3D rotating system (right) and the reduced model including $(0,0,0)$ and $(0,\pm,\pm)$ interactions (left).

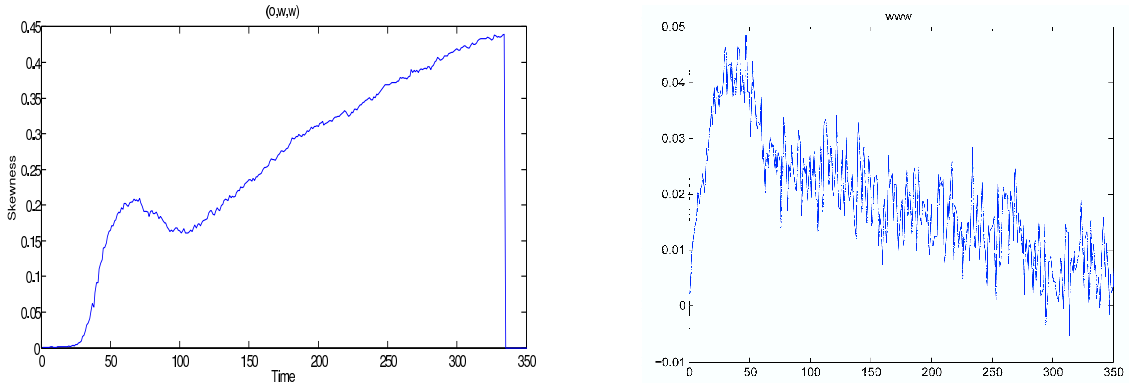

Figure 22: Skewness of vorticity vs time for the reduced models $(0, \pm, \pm)$ (right) and $(\pm, \pm, \pm)$ interactions (left).

(and all permutations) is more efficient at transferring energy to large scales than the full system. Notice the higher energy level in the right panel of each plot showing energy in time (Figure 19) and single-time spectra (Figure 20) for the mode $(0,0,0) + (0, \pm, \pm)$. The 2D nature of the large scale flow ($k < k_f = 24$) and the scaling of the energy spectrum $E(k) \approx E(k_z = 0) \propto k^{-3}$ is well captured by the reduced model. Since the only difference between the two systems is the presence of the three-wave interactions in the full system, it is immediately evident that three-wave interactions inhibit the transfer of energy into large-scale 2D flows. Figure 21 shows that the vorticity skewness associated with the model $(0,0,0)+(0, \pm, \pm)$ is slightly more positive than the vorticity skewness of the full equations for long times, indicating that the reduced model and full equations both generate similarly strong coherent cyclones. Finally, Figure 22 compares the vorticity skewness associated with $(0, \pm, \pm)$ interactions in isolation (right) and $(\pm, \pm, \pm)$ interactions in isolation. One sees that the $(0, \pm, \pm)$ interactions generate positive skewness, although the magnitude is smaller than the reduced model $(0,0,0) + (0, \pm, \pm)$. On the right, one also sees that $(\pm, \pm, \pm)$ interactions in isolation lead to skewness near zero for long times. Hence, the conclusions are that (i) $(0, \pm, \pm)$ interactions are responsible for the cyclone/anticyclone asymmetry in favor of cyclones, (ii) the reduced model $(0,0,0) + (0, \pm, \pm)$ is more efficient than the full system for the generation of large-scale coherent cyclones from random forcing at small scales, and (iii) the $(\pm, \pm, \pm)$ interactions inhibit the formation of large-scale coherent cyclones.

7. Effects of the hydrostatic approximation on energy redistribution in rotating and stratified flows: Susan Kurien, Jai Sukhatme and Leslie Smith.

This work is in progress. Our results for low resolution simulations are summarized below, however, it is clear that we need much higher resolutions to thoroughly understand the differences between hydrostatic and Boussinesq simulations in small aspect ratio domains. For example, consider two simulations with an isotropic energy source at intermediate scales, one with $H/L = 1$ and the other with $H/L = 1/10$. A minimal resolution at small geophysical values of the Rossby and Froude numbers $<< 1$ for the benchmark simulation with $H/L = 1$ in a 2π periodic domain would be 256^3. Now consider increasing the horizontal length scale by a factor of 10 such that the domain becomes $20\pi \times 20\pi \times 2\pi$ with $H/L = 1/10$. Then in order to maintain integrity of the isotropic forcing and the same resolution in all directions, the resolution for the small aspect ratio run with $H/L = 1/10$ should be $2,560 \times 2,560 \times 256$. At low resolutions and low aspect ratios, inadequate resolution may lead to spurious growth of modes that are biased by the inadvertently anisotropic

forcing. We have been awarded 25,000,000 processor hours on the IBM Blue Gene/P at Argonne National Laboratory through the DOE Office of Science program Innovative and Novel Computational Impact on Theory and Experiment (INCITE).

Starting from the Boussinesq equations for rotating and stratified flow, the hydrostatic approximation assumes vertical accelerations are negligible, and thus that the vertical motion is always in a state of hydrostatic balance. Then the dispersion relation for wave frequencies is modified from the Boussinesq expression

$$\sigma^B(\mathbf{k}) = \pm\frac{(f^2k_z^2 + N^2k_h^2)^{1/2}}{k} \tag{14}$$

to become

$$\sigma^H(\mathbf{k}) = \pm\frac{(f^2k_z^2 + N^2k_h^2)^{1/2}}{k_z}. \tag{15}$$

where k_z, k_h are the vertical and horizontal components of the wavevector, respectively, and k is the magnitude of the wavevector $\mathbf{k}$. In essence, with the Boussinesq approximation $\sigma^B = \{0, [-N, -f], [f, N]\}$ (as for the complete rotating stratifed fluid equations after removing acoustic waves) whereas by imposing hydrostatic balance $\sigma^H = \{0, [-\infty, -f], [f, \infty]\}$. Usually the hydrostatic approximation is justified by invoking a large disparity amongst the vertical (L) and horizontal (H) scales of motion, i.e. $H/L << 1$. However, (15) shows that, in order to avoid the generation of "spurious" high frequcency waves, one actually requires $k_h << k_z$. The implication is that if the wavenumber spacing is given by $\Delta k_x = \Delta k_y = 2\pi/L$, $\Delta k_z = 2\pi/H$, then $N_x \leq \sqrt{2}L/H$ is required to satisfy $k_h << k_z$. In other words, increasing the horizontal resolution (i.e. increasing N_x) for a specified aspect ratio will result in the generation of the aforementioned spurious high frequency inertial-gravity waves. Note that increasing N_x to resolve smaller scales of motion while artificially truncating the frequencies to lie between $[f, N]$ is likely to result in a violation of basic conservation laws — indeed, this is one of the points we are presently examining. For example, Fig. 23 shows the effect of higher frequency waves on the total energy distribution for hydrostatic simulations in a periodic box. The parameter values are $N/f = 25$, $Fr = U/(L_f N) = 0.2$ and $L/H = 25$, where U, L_f are the characteristic velocity and length scales of the force. The force is 3D, isotropic, white in time, with a gaussian two-point spatial correlation function peaked at $k_f = 43$. A hyperviscosity is used in order to allow for a range of scales where viscous effects are negligible. The hydrostatic simulations are purposely "over-resolved" in the sense that $k_h << k_z$ is violated. We allow successively more spurious high-frequency inertial-gravity waves: the three different simulations allow inertial-gravity waves with frequencies in the range $[f, N]$ (curve with dots), $[f, 4N]$ (curve with stars) and $[f, 8N]$ (curve with open circles). As we allow the higher unphysical frequencies to enter the simulation, the energy transfer is inhibited with the spectrum tending towards isolated peaks at multiples of the forcing frequency.

Figure 24 compares total energy spectra for a hydrostatic simulation that satisfies the constraint $k_h << k_z$ with resolution $32 \times 32 \times 64$ to a Boussinesq simulation with resolution $180 \times 180 \times 64$. The parameters and forcing are the same as for Fig. (23): $N/f = 25$, $L/H = 25$, $Fr = 0.2$, $k_f = 43$. One sees that the hydrostatic interactions are not sufficient to extract energy from the forced modes, whereas the Boussinesq interactions transfer energy from the forced modes to both larger and smaller scales. The higher horizontal resolution is necessary for the nonlinear transfer to occur, but as discussed above, higher resolution in the hydrostatic runs violates the condition $k_h << k_z$ under which the hydrostatic equations are derived. In the Boussinesq run, the energy

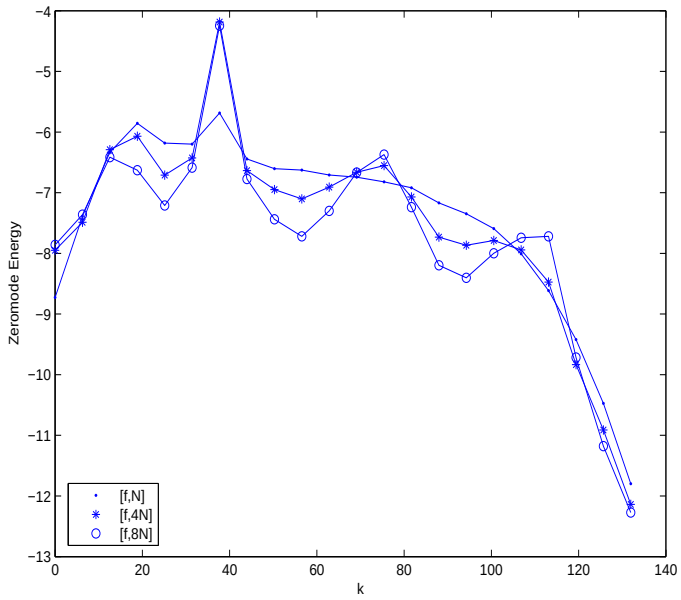

Figure 23: The total energy at equilibrium in hydrostatic simulations for $N/f = 25$ and with forcing parameter $k_f = 43$. All of these hydrostatic simulations are "over-resolved" (in the sense that $k_h << k_z$ is violated) with $L/H = 25$ and resolution $180 \times 180 \times 64$. The spurious high-frequency waves (curves with stars and circles) inhibit energy transfer from the peak forced wavenumber to other wavenumbers that are not integer multiples.

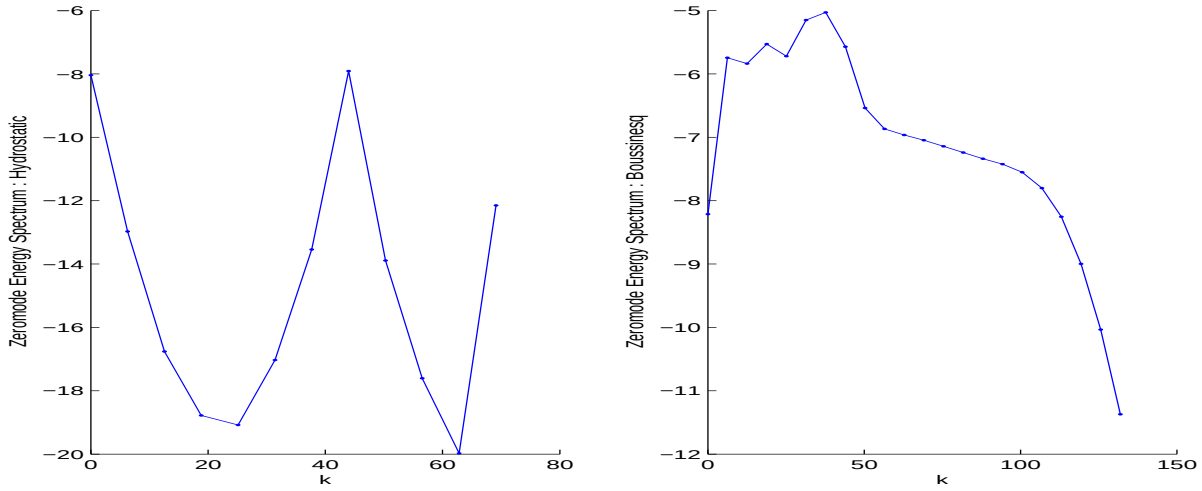

Figure 24: Total energy in the hydrostatic (left panel) and Boussinesq (right panel) runs with $N/f = 25$, $L/H = 25$ and $k_f = 43$. The hydrostatic run is consistent with the assumptions used to derive the hydrostatic approximation: $L/H = 25$ and the resolution is $32 \times 32 \times 64$, i.e. $N_x < \sqrt{2}L/H$. The Boussinesq run is at a resolution of $180 \times 180 \times 64$.

spectrum for intermediate scales appears to have a well-defined scaling that may indicate the possibility of inertial-range dynamics.

Further, a subtlety that comes in the Boussinesq equations is that they admit two distinct limits in terms of stratification and rotation. Specifically, measuring the strength of stratification and rotation in terms of the smallness of the Froude ($Fr = UL/N$) and Rossby ($Ro = UL/f$) numbers respectively, the two limits are (a) Fr small, $Ro \sim O(1)$ and (b) Fr, Ro both small. These correspond to vertically sheared horizontal flows (VSHF) and quasi-geostrophic (QG) flows respectively (Embid & Majda, 1998). If one imposes hydrostatic balance, i.e. if $H/L << 1$, then the first limit is difficult to achieve since a small Fr implies a small Ro, meaning that the only limit accessible is that of quasigeostrophy.

8. Local and nonlocal dispersive turbulence. Jai Sukhatme and Leslie Smith

The results of this research have been appeared in Sukhatme, J. & Smith, L.M., Local and nonlocal dispersive turbulence, *Phys. Fluids* **21**, 056603, 2009.

In the 2D context, simple model equations that possess advection and dispersion include the familiar barotropic beta plane equation (Rhines, 1975) and the dispersive surface quasigeostrophic (SQG) equations (Held, Pierrehumbert, Garner and Swanson, 1995). We look at an extended family (that includes the aforementioned examples as members) of dispersive active scalars. Our family is a simple dispersive generalization of the family of 2D turbulence models introduced in Pierrehumbert, Held & Swanson (1994). Specifically, in a 2D periodic setting we consider

$$\begin{aligned} &\frac{D\theta}{Dt} + \frac{1}{\epsilon}\frac{\partial \psi}{\partial x} = 0 \ ; \ (u,v) = (-\frac{\partial \psi}{\partial y}, \frac{\partial \psi}{\partial x}) \\ &\text{where} \ \ \hat{\theta}(k_x, k_y, t) = -(k^2)^{\alpha}\hat{\psi}(k_x, k_y, t) \end{aligned} \tag{16}$$

where D/Dt denotes the 2D material derivative and ϵ is a non-dimensional parameter. Note that in real space θ and ψ above are related via a suitable (pseudo-) differential operator, i.e. $\theta = -(-\triangle)^{\alpha}\psi$ where $\triangle$ is the 2D Laplacian. For the beta plane equations we have $\alpha = 1$, θ is the vorticity field, and ϵ corresponds to the Rhines number $Rh = U/(\beta L^2)$. In the dispersive SQG case $\alpha = 1/2$, θ now represents the buoyancy (or potential temperature), and $\epsilon = U/(\Lambda L)$. Physically, of course we are dealing with very different scenarios wherein β is the ambient planetary gradient of the vorticity while Λ is the background surface buoyancy gradient. Apart from $\alpha = 1, 1/2$, there exist other members of this family that have physical interpretations, but, from a broader perspective, the entire family is well defined, and we expect that varying α would provide greater insight into the interplay between advection and dispersion.

Before considering the effect of dispersion, we examine the influence of α. To obtain a feel for the locality of the interactions, we shut off the linear dispersive term in (16) and consider a simple numerical exercise involving the evolution of a smooth θ ring. As is seen in Fig. (25), the deformation of the ring is more physically local for smaller α. Given that $\hat{\psi}(\vec{k}) = -\hat{\theta}(\vec{k})/k^{2\alpha}$, as α increases, one sees that only the small k features of θ and ψ remain dynamically active. As a result, for larger α, smaller scale features of the scalar field are for all purposes driven in a passive manner. In fact in the limit $\alpha \to \infty$, only the wavenumber one ($k = 1$) component of θ and ψ is coupled, and in essence, we end up with the problem of passive advection via a large-scale smooth flow.

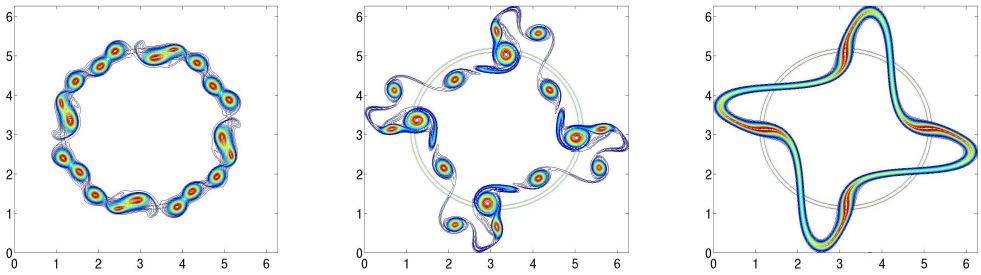

Figure 25: Non-dispersive evolution of θ rings. From left to right, $\alpha = 0.5, 1$ and 1.5 respectively. Quite clearly, as α decreases the deformation of the ring is more local in character.

In contrast, the case of small α is markedly different. Specifically $(\hat{u}, \hat{v}) = (\mathrm{i}k_y\hat{\theta}/k^{2\alpha}, -\mathrm{i}k_x\hat{\theta}/k^{2\alpha})$ results in a transition at $\alpha = 1/2$ (when the scalar and velocity fields have similar scales) where for $\alpha < 1/2$ — even though ψ remains a smoothened form of θ — the velocity fields are in fact of a finer scale than the advected scalar field.

In a 2D periodic domain, much like their non-dispersive counterparts, (16) conserves energy $E = \int_{\mathbf{D}} \psi\theta$ and enstrophy or "θ-variance" $\mathcal{E} = \int_{\mathbf{D}} \theta^2$. In fact, continuing with the non-dispersive case; following arguments for the 2D Euler equations (Kraichnan 1967), it is expected that the energy primarily flows to large scales while the θ-variance is transferred to small scales. If we consider a simple Fjortoft-like estimate, i.e. the transfer of energy out of scale k_1 into scales k_0, k_2 (s.t. $k_0 = k_1/2\alpha$ and $k_2 = 2\alpha k_1$), we have $E_0 = E_1 \times \{(2\alpha)^{2\alpha}/[1 + (2\alpha)^{2\alpha}]\}$; i.e. the more nonlocal the situation ($\alpha > 0.5$), the larger is the fraction of the energy (enstrophy) transferred to large (small) scales. Curiously such a monotonic statement does not hold for increasing locality, i.e. for $\alpha < 0.5$. Keeping in mind that for $\alpha < 0.5$, k_0 is the small scale, as is seen in Fig. (26), a larger fraction of enstrophy (energy) is always transferred into the small (large) scale, but for $\alpha < 0.5$, there is a local extremum $\alpha = \alpha_* = \exp\{-1\}$ for which enstrophy (energy) transfer to the small (large) scale (k_2) is actually maximized. Also note that, for $\alpha > 0.5$, not only is a larger fraction of the enstrophy (energy) transferred to small (large) scales, the exchange involves scales that are progressively further apart, i.e. we have a spectrally nonlocal transfer. It is known that forward (inverse) enstrophy (energy) transfer in 2D turbulence (i.e. $\alpha = 1$) is spectrally nonlocal (weakly nonlocal) , and is supported by the Fjortoft estimate that suggests a monotonic increase in spectral non-locality for $\alpha > 0.5$.

To develop a feel for the dependence of the geometry of an emergent scalar field on α, we continue with non-dispersive simulations, though now from spatially un-correlated initial data chosen from a Gaussian distribution with unit variance. Given the presence of an inverse transfer of energy, we expect coherent structures to emerge from this un-correlated initial condition. In fact, given the similar scales of the velocity and scalar fields for smaller α we do not expect the scalar field to undergo much stretching and folding, while for large α we expect repeated events of this sort leading to a filamentary scalar field — much like the fate of a small-scale passive blob when advected by a large-scale smooth flow — due to the implicit large-scale strain (via the large scale-separation between θ and ψ). These expectations are confirmed in Fig. (27) which shows the initial condition and the emergent scalar field for $\alpha = 0.5$ and 2 respectively.

When the dispersive term is included, the linearized form of (16) supports waves with the

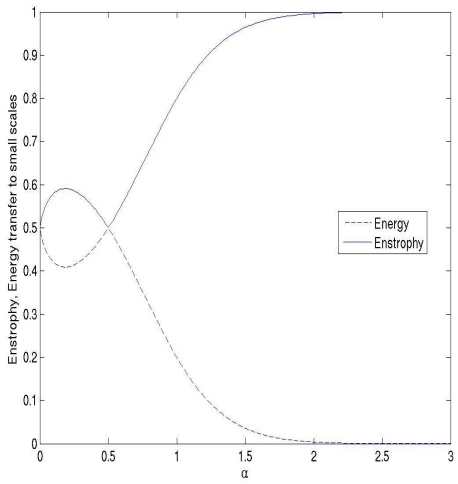

Figure 26: Energy and Enstrophy transfer into the small scales. Note that the three interacting scales are $k_0 = k_1/(2\alpha), k_1$ and $k_2 = 2\alpha k_1$ and hence the large and small scales flip at $\alpha = 0.5$. In all cases, a larger (smaller) fraction of the enstrophy (energy) is transferred into the smaller scale.

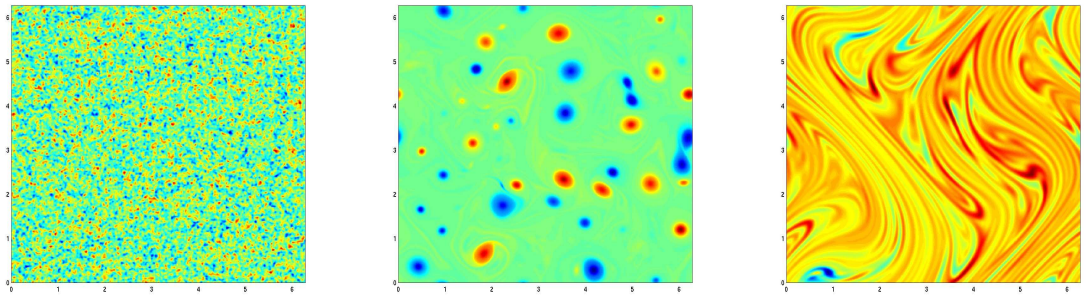

Figure 27: The first panel is the spatially un-correlated initial condition (smoothened via a diffusive stencil). The second and third panels show the emergent scalar field for $\alpha = 0.5$ and 2 respectively. Quite clearly, for $\alpha = 0.5$ we have a field composed of coherent θ eddies while for $\alpha = 2$ we obtain a filamentary geometry reminiscent of a passive field when subjected to large-scale advection.

dispersion relation

$$\omega(\vec{k}) = -\frac{k_x}{\epsilon k^{2\alpha}} \quad ; \quad \text{where} \quad \vec{k} = (k_x, k_y) \tag{17}$$

It is interesting to note that, for $\alpha = 0.5$, (17) gives $0 \leq |\omega(\vec{k})| \leq 1/\epsilon$. For $\alpha < 0.5, |\omega| \to \infty$ for $k_y = 0, k_x \to \infty$, whereas for $\alpha > 0.5, |\omega| \to \infty$ for $k_y = 0, k_x \to 0$. Quite clearly the frequencies have a very different dependence on wavenumber when $\alpha <, =$ or > 0.5. In fact, an important feature of the beta plane equations (which is true for all $\alpha > 0.5$) that $|\omega(\vec{k})|$ increases for large scales is no longer true for $\alpha \leq 0.5$; in fact, for $\alpha < 0.5$ the smaller scale features have larger frequencies.

Considering an initial value problem, the original deduction of anisotropic fields by Rhines (1975), in the context of the beta plane equations was based on the dual constraint of an upscale transfer of energy along with the tendency of resonant triads to move energy into small frequencies (Hasselmann, 1967). Indeed, there are two pieces of the Rhines argument : (i) energy moving to large scales as a result energy/enstrophy conservation, and (ii) the importance of resonant triads in energy transfer with dispersive modulation of the advective nonlinearity. In the context of the general dispersion relation (17), for isotropic structures, $k_x \sim k_y \sim k$ we have

$$|\omega| = \frac{1}{\epsilon 2^{\alpha}} \frac{1}{k^{2\alpha-1}}. \tag{18}$$

Hence for $\alpha > 0.5$, moving to large scales, i.e. for decreasing k we encounter larger frequencies. Therefore, to satisfy the dual constraints, Rhines (1975) suggested that the system would spontaneously generate anisotropic structures; further examining (17) shows that these constraints are satisfied for $k_y \neq 0, k_x/k_y \ll 1$. Also, when considering energy transfer into large scales, i.e. $k < p, q$, interactions that fall in the aforementioned anisotropic category are in fact near-resonant. In essence we have an anisotropic streamfunction that results in predominantly zonal flows (i.e $u \approx u(y,t)$). Though note that for $\alpha < 0.5$, decreasing k implies smaller frequencies, therefore it is possible to maintain isotropy while simultaneously transferring energy to large scales and small frequencies. Hence, for $\alpha < 0.5$, the dual constraints do not nessecitate the formation of a dominant of zonal flow. Note that this does not imply zonal flows cannot form for $\alpha < 0.5$, in fact, substituting an expansion of the form $\psi = \psi^0 + \epsilon\psi^1 ...$, the $O(1/\epsilon)$ balance in (16) yields $\partial\psi^0/\partial x = 0 \Rightarrow u^0 = u^0(y,t), v^0 = 0$. Of course, this expansion doesn't imply any control over the higher order terms, but irrespective of α, at order zero, it indicates the possibility of zonal flow formation.

To examine the nature of emergent flows for differing locality, we perform numerical simulations with spatially un-correlated initial data as shown in the first panel of Fig. (27). Setting $\epsilon = 0.1$, the scalar and zonal component of the velocity fields for $\alpha = 0.25, 1$ and $\alpha = 1.25$ are shown in Fig. (28), quite clearly for $\alpha > 0.5$ we have, what might be termed a coherent zonal flow i.e. $u \approx u(y,t)$, while for $\alpha = 0.25$, u is still a function of both spatial co-ordinates. Note that, in accord with Fig. (23), the flows are broader and of smaller magnitude for increasing α.

With regard to the mathematical aspects of (16), $\alpha = 0.5$ is known to be special in the sense that it represents an open problem with regard to global regularity of non-dissipative solutions (see for example Constantin, Majda & Tabak 1994 for an analogy between front formation in SQG and finite time singularities in the 3D Euler equations). In fact, present estimates for well behaved

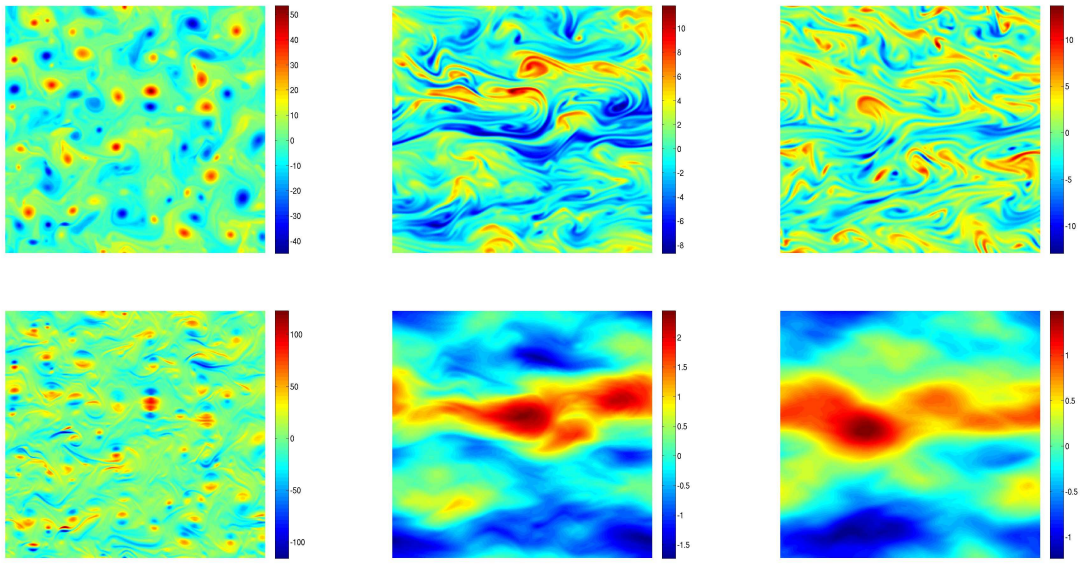

Figure 28: θ, u fields for $\alpha = 0.25, 1$ and 1.25 in the upper and lower panels respectively. In all cases $\epsilon = 0.1$. Note the finer scale of the flow as compared to the scalar field when $\alpha = 0.25$. Further for increasing α, we see $u \approx u(y,t)$ i.e. we obtain coherent zonal flows.

solutions require dissipation of the form $\triangle^\rho$ with $\rho = 0.5$ for both, the non-dispersive and dispersive cases (Kiselev, Nazarov & Volberg 2007, Kiselev & Nazarov 2008). Unfortunately, regularity results for $0.5 < \alpha < 1$ are presently un-settled. It is unclear if the difficulty in achieving regularity (by present techniques) arises abruptly at $\alpha = 0.5$ or whether one requires gradually stronger dissipation as α decreases from unity. Ultimately, in our opinion it might be interesting to delineate the nature of the (α, ρ) "regularity curve" for $0 < \alpha \leq 1$, and as $\alpha = \exp\{-1\}$ is a local maximum for enstrophy transfer to small scales, we feel this makes it a good candidate for investigating the breakdown of smooth initial conditions.

7. Oceanic mixing forced by remote wind forcing through internal gravity wave breaking: The single wave case, Wei Liu, Zhengyu Liu, Francis Bretherton, Leslie Smith, Christ Rotland, Hao Lu

A paper is to be submitted to Journal of Physical Oceanography

Interior ocean mixing forced by surface wind forcing is studied in the idealized case of surface forcing internal gravity wave breaking. The breaking of internal gravity waves by convective instability is studied by direct numerical simulation (DNS) based on a newly-developed pesudospectral model, which is more accurate than a finite difference code. On a two-dimensional fluid dynamics in the vertical (x, z)-plane, the Navier–Stokes equations in the Boussinesq approximation can be written in terms of the streamfunction and fluctuating density fields $\rho = (g/\rho_0)\tilde{\rho}$ as

$$\frac{\partial \nabla^2 \psi}{\partial t} + J(\nabla^2 \psi, \psi) = \frac{\partial \rho'}{\partial x} + \upsilon \nabla^2 \psi$$

$$\frac{\partial \rho}{\partial t} + J(\rho, \psi) = -N^2 \frac{\partial \psi}{\partial x} + \kappa \nabla^2 \rho$$

where v is the kinematic viscosity coefficient and κ the density diffusion coefficient. $J(A,B) = (\partial A/\partial x)(\partial B/\partial z) - (\partial A/\partial z)(\partial B/\partial x)$ is the Jacobian operator.

Different from previous studies, this model employs top boundary forcing to generate a monochoromatic two-dimensional wave, which allows it to simulate the remote breaking process in the progressive wave. For simplicity here, the effects of mean flow is excluded. Isopyncal overturning and associated convective instability arises when the primary wave steepness $s = 0.75 - 0.79$, below the conventional critical value $s = 1$ (Fig.7.1). Due to dissipation and mixing effect in modifying the mean stratification, the surface forcing effect induced mixing is limited in the depth shallower than the wave propagation (Fig.7.1). Furhtermore, the critical steepness of ~0.75 is insensitive to the forcing frequency (not shown). Energy spectrums remain unchanged at the onset of isopycnal overturning and most high harmonics are not developed until the primary wave steepness increases to beyond $s = 1$. Energy is more apt to transfer from the primary wave to higher harmonics (smaller scale) with slower forcing frequency.

Further analysis shows that the wave breaking is caused by two mechanisms: the convective instability and shear instability. The two types of instability occurred in preferred phase, as indicated schematically. Convective instability occurs at the phase of 0.5pi, while shear instability occurs at 0 and pi, as shown schematically in Fig.7.2.

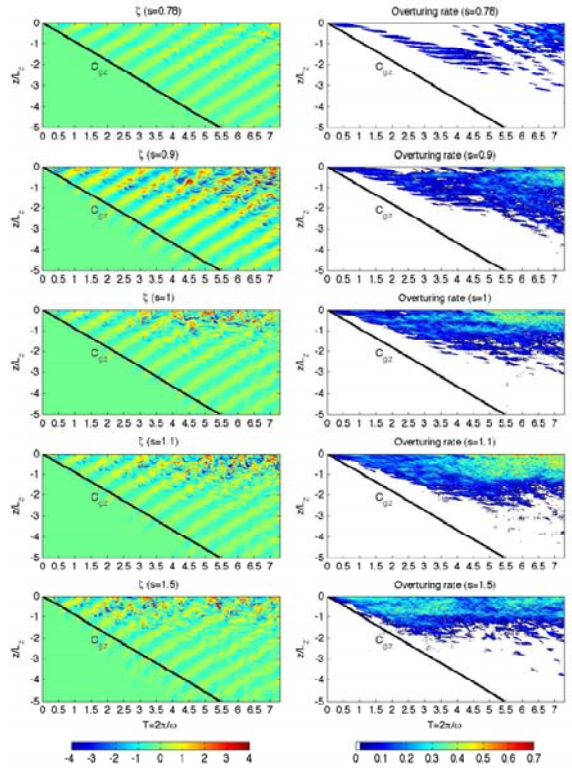

Figure 7. 1. Depth-time diagram of (a) vorticity and (b) density at $x = -0.2L_x$. For various forcing steepness *s*. This figure shows how the surface wave forcing generates breaking and mixing remotely away from the surface forcing. But the depth of mixing is confined shallower than the propagation wave.

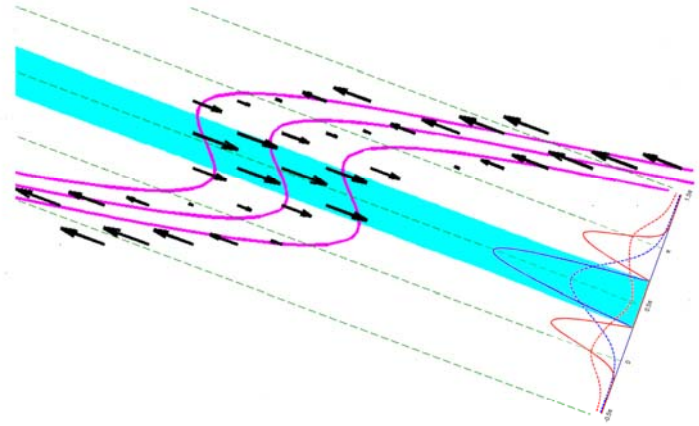

Figure 7. 2. Schematic diagram of instability phase range, blue shading near 0.5pi indicate the strongest overturning and therefore most likely convective instability, while the green dashed lines along 0 and pi are the region of strongest shear and in turn shear instability.

The mixing effect on mean stratification is seen in the example in Fig.7.3. It is seen that heavier fluid is moved to the surface while light fluid in the subsurface (Fig.7.3b), obviously the result of mechanical mixing caused by the surface wind. The induced eddy mixing coefficient reaches it maximum in the top half wave length and then decays downward (Fig.7.3c). The mixing coefficient generally increases with the steepness of the forcing wave (Fig.7.4).

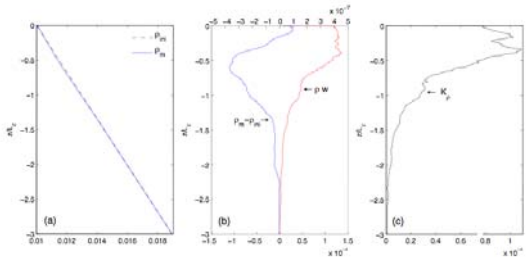

Figure 7. 3. An example of vertical profile of (a) total density, (b) density anomaly and buoyancy flux, and (c) mixing coefficient.

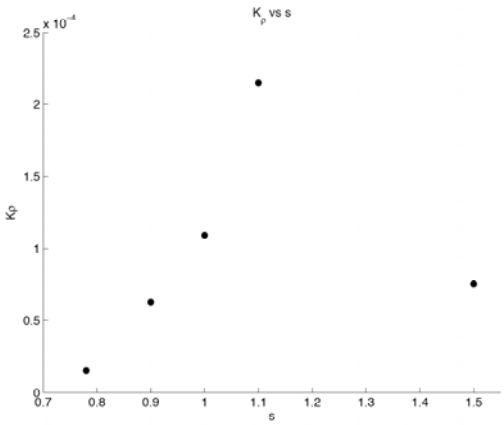

Figure 7. 4. Eddy mixing coefficient as a function of forcing wave steepness.

This study demonstrates explicitly that surface wind can indeed generate significant remote mixing in the subsurface ocean. However, for a single wave, unrealisitcally strong surface forcing is needed to generate mixing. We speculate that in the real world random wave interactions produce spontaneous mixing and the GM spectrum. This will be studied in the future.